

VASSO: Variance Suppression for Sharpness-Aware Minimization

Bingcong Li, Yilang Zhang, and Georgios B. Giannakis

Abstract—Sharpness-aware minimization (SAM) has well-documented merits in enhancing generalization of deep neural network models. Accounting for sharpness in the loss function geometry, where neighborhoods of ‘flat minima’ heighten generalization ability, SAM seeks ‘flat valleys’ by minimizing the maximum loss provoked by an *adversarial* perturbation within the neighborhood. Although critical to account for sharpness of the loss function, in practice SAM suffers from ‘*over-friendly* adversaries,’ which can curtail the outmost level of generalization. To avoid such ‘friendliness,’ the present contribution fosters stabilization of adversaries through *variance suppression* (VASSO). VASSO offers a general approach to *provably* stabilize adversaries. In particular, when integrating VASSO with SAM, improved generalizability is numerically validated on extensive vision and language tasks. Once applied on top of a computationally efficient SAM variant, VASSO offers a desirable generalization-computation tradeoff.

Index Terms—Generalization, sharpness-aware minimization, deep neural networks, optimization

1 INTRODUCTION

Deep neural network (DNN) models have advanced the notion of “learning from data,” and they have markedly improved performance across various application tasks in vision and language [1, 2]. Unfortunately, their overparametrization renders them prone to overfit on training data [3], which hampers their generalization ability on unseen data. This shortcoming has been underscored in practice, and points to a gap in evaluating performance of training.

Common approaches to improving generalizability of DNNs include regularization and data augmentation [4]. While it is a default choice to integrate regularization such as weight decay and dropout when training in practice, these methods are often insufficient for DNNs, especially when dealing with complicated network architectures [5]. Another line of efforts resorts to suitable optimization schemes, attempting to find a generalizable local minimum. For example, stochastic gradient descent (SGD) outperforms Adam on certain overparameterized problems owing to its convergence to maximum margin solutions [6]. Decoupling weight decay from Adam has been empirically seen to facilitate generalizability for many language tasks [7]. Unfortunately, the underlying mechanism promoting generalization remains elusive, and whether the generalization merits carry over to other intricate learning problems calls for extra theoretical investigations.

Our main focus is sharpness-aware minimization (SAM) – a compelling optimization approach that facilitates state-of-the-art generalizability by exploiting areas of sharpness and flatness in the loss landscape [5, 8]. A high-level interpretation of sharpness is how markedly the loss fluctuates in the neighboring parameter space. Large-scale empirical studies have shown that sharpness-based measures highly correlate with generalization [9], and flat minima improve generalizability [5, 8, 10]. This can be conceptually understood using Fig. 1, where the test loss only slightly

increases in flat valleys under distributional shifts. A number of approaches have embraced sharpness to boost generalization. The work in [10] suggests that the batchsize of SGD impresses solution flatness. Entropy SGD leverages the local entropy in search of a flat valley [11]. Different from prior works, SAM induces flatness by explicitly minimizing the *adversarially* perturbed loss, defined as the maximum loss of a neighboring area. Through such a perturbed loss, SAM has boosted generalization in various vision and language tasks [5, 12]. The mechanism behind SAM’s success has been theoretically investigated based on arguments of implicit regularization; see e.g., [13, 14, 15].

The notion of a perturbing adversary, or the *adversary* for short, is central to SAM’s improved generalization because it effectively measures sharpness through the loss difference with the original model [8, 16, 17]. In practice however, accounting for sharpness is undermined by what can be viewed as a *friendly adversary*. Confined by the stochastic linearization for computational efficiency, SAM’s adversary only captures the sharpness for a particular minibatch, and can become a friend on other data samples. Because ‘global sharpness’ is not approached accurately, the friendly adversary challenges SAM from attaining its utmost generalizability. To overcome this challenge, the present work advocates variance suppression (VASSO¹) to alleviate ‘friendliness’ by stabilizing adversaries. VASSO is a general approach that can be seamlessly integrated with SAM variants to theoretically and numerically demonstrate gain in generalization. This work focuses particularly on two of the most valuable use cases.

The first one is to integrate VASSO with vanilla SAM. The resultant algorithm, also referred to as VASSO, has a *provable* stabilized adversary that showcases favorable numerical performance over SAM for a wide spectrum of deep learning tasks.

The second application of VASSO manifests in trading off generalization for computational efficiency. At one extreme, the drastically improved generalization of SAM incurs the cost of two backpropagations per iteration. The opposite extreme is SGD, where low computational cost comes at the price of a moderate

B. Li is with Department of Computer Science at ETH Zürich, 8092 Zürich, Switzerland. Email: bingcong.li@inf.ethz.ch.

Y. Zhang and G. B. Giannakis are with the Department of Electrical and Computer Engineering, University of Minnesota, Minneapolis, MN 55455, USA. Emails: {zhan7453, georgios}@umn.edu.

Most of this work was performed when B. Li was at the Univ. of Minnesota.

1. VASSO coincides with the Greek nickname for Vasiliki.

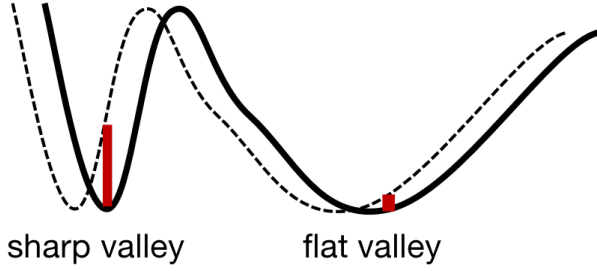


Fig. 1. Intuition on why flat minima boost generalization. Solid (dotted) curve denotes training (test) loss. The red bar indicates the gap between training and test loss. Clearly, this gap is smaller on flat valleys.

level of generalization. Recent research has enriched this tradeoff by developing lightweight SAM variants. For instance, LookSAM computes the extra stochastic gradient once every few iterations, and reuses it in a fine-grained manner to approximate the additional gradient [18]. ESAM obtains its adversarial vector based on stochastic weight perturbation, and further saves computation by selecting a subset of the minibatch data for gradient computation [19]. The computational burden of SAM can also be lowered by switching between SAM and SGD following a predesigned schedule [20], or adaptively as in [21]. SAF connects SAM with distillation to reduce computational complexity [22]. However, most of these works reuse the stochastic linearization of SAM, which reduces their ability to cope with friendly adversaries, and prevents them from attaining a desirable generalization-computation tradeoff. To this end, VASSO is combined here with a computationally efficient SAM variant [20]. For a prescribed computational budget, the resultant algorithm termed efficient VASSO (eVASSO), leads to markedly improved generalization.

All in all, our contributions can be summarized as follows.

- ❖ A *friendly adversary* is identified as an obstacle challenging generalizability of SAM. Experiments demonstrate that it can even nullify the generalization benefits.
- ❖ *Variance suppression* is developed to handle this issue by stabilizing adversaries. The theoretically guaranteed stability promotes refined global sharpness estimates, and thus alleviates the impact of friendly adversaries. The merits of VASSO are demonstrated also experimentally on tasks such as image classification, domain generalization, label noise, and neural machine translation.
- ❖ VASSO improves the generalization-computation trade-off when integrated with computationally efficient SAM variants such as eSAM. For the same generalization level, the resultant approach, eVASSO, saves 57% and 70% computational overhead relative to eSAM and SAM, respectively.

This work broadens and innovates over [23] in three directions: (i) a computationally efficient algorithm is developed and analyzed to desirably trade off generalization for computation in sharpness-aware minimization; (ii) numerical tests incorporate more challenging tasks such as domain generalization; and (iii) further elaboration and insights are included to improve intuition.

Notation. Bold lowercase (capital) letters denote column vectors (matrices); $\|\mathbf{x}\|$ stands for ℓ_2 norm of vector \mathbf{x} ; and $\langle \mathbf{x}, \mathbf{y} \rangle$ is the inner product of \mathbf{x} and \mathbf{y} . $\mathbb{S}_\rho(\mathbf{x})$ denotes the surface of a ball with radius ρ centered at \mathbf{x} , i.e., $\mathbb{S}_\rho(\mathbf{x}) := \{\mathbf{x} + \rho \mathbf{u} \mid \|\mathbf{u}\| = 1\}$.

Algorithm 1 Generic form of SAM

```

1: Initialize:  $\mathbf{x}_0, \rho$ 
2: for  $t = 0, \dots, T - 1$  do
3:   Sample a minibatch  $\mathcal{B}_t$ 
4:   Define stochastic gradient on  $\mathcal{B}_t$  as  $\mathbf{g}_t(\cdot)$ 
5:   Find  $\boldsymbol{\epsilon}_t \in \mathbb{S}_\rho(\mathbf{0})$  via stochastic linearization; e.g.,
6:     // (5) for VASSO, or (3) for SAM
7:   Calculate stochastic gradient  $\mathbf{g}_t(\mathbf{x}_t + \boldsymbol{\epsilon}_t)$ 
8:   Update model via  $\mathbf{x}_{t+1} = \mathbf{x}_t - \eta \mathbf{g}_t(\mathbf{x}_t + \boldsymbol{\epsilon}_t)$ 
9: end for
10: Return:  $\mathbf{x}_T$ 

```

2 THE KNOWN, THE GOOD, AND THE CHALLENGE

This section starts with a recap of SAM (i.e., the known), followed by refined analyses and SAM's convergence upshot (i.e., the good). Next, the notion of a *friendly adversary* that confines generalizability is elaborated and illustrated numerically.

2.1 The known

Aiming at a minimum with a flat basin, SAM enforces small loss around the entire neighborhood in the parameter space [8]. This idea is formulated as a minimax problem

$$\min_{\mathbf{x}} \max_{\|\boldsymbol{\epsilon}\| \leq \rho} f(\mathbf{x} + \boldsymbol{\epsilon}) \quad (1)$$

with ρ denoting the radius of the considered neighborhood, and $f(\mathbf{x}) := \mathbb{E}_{\mathcal{B}}[f_{\mathcal{B}}(\mathbf{x})]$ the possibly nonconvex objective, where \mathbf{x} is the neural network parameter, and \mathcal{B} is a random minibatch of data. Formulation (1) captures the implicit sharpness measure $\max_{\|\boldsymbol{\epsilon}\| \leq \rho} f(\mathbf{x} + \boldsymbol{\epsilon}) - f(\mathbf{x})$, which effectively drives the optimization trajectory towards the desirable flat valley [17].

The inner maximization in (1) has a natural interpretation as finding an *adversarial model* for \mathbf{x}_t , where t denotes the iteration index. Critical as it is, such an adversary prompts *stochastic linearization* to avoid full gradient computation, that is,

$$\begin{aligned} \boldsymbol{\epsilon}_t &= \arg \max_{\|\boldsymbol{\epsilon}\| \leq \rho} f(\mathbf{x}_t + \boldsymbol{\epsilon}) \stackrel{(a)}{\approx} \arg \max_{\|\boldsymbol{\epsilon}\| \leq \rho} f(\mathbf{x}_t) + \langle \nabla f(\mathbf{x}_t), \boldsymbol{\epsilon} \rangle \\ &\stackrel{(b)}{\approx} \arg \max_{\|\boldsymbol{\epsilon}\| \leq \rho} f(\mathbf{x}_t) + \langle \mathbf{g}_t(\mathbf{x}_t), \boldsymbol{\epsilon} \rangle \end{aligned} \quad (2)$$

where linearization (a) relies on the first-order Taylor expansion of $f(\mathbf{x}_t + \boldsymbol{\epsilon})$ that is typically accurate when choosing ρ small. Consider next replacing $\nabla f(\mathbf{x}_t)$ in (b) with a stochastic gradient $\mathbf{g}_t(\mathbf{x}_t)$ on minibatch \mathcal{B}_t to reduce the computational burden of $\nabla f(\mathbf{x}_t)$. Catalyzed by the stochastic linearization in (2), it is possible to express SAM's adversary in closed form as

$$\boxed{\text{SAM: } \boldsymbol{\epsilon}_t = \rho \frac{\mathbf{g}_t(\mathbf{x}_t)}{\|\mathbf{g}_t(\mathbf{x}_t)\|}} \quad (3)$$

SAM then adopts the adversarial stochastic gradient $\mathbf{g}_t(\mathbf{x}_t + \boldsymbol{\epsilon}_t)$ to update \mathbf{x}_t per SGD fashion. A step-by-step implementation is listed in Alg. 1, where the means to find an adversary in lines 5 and 6 is presented in a generic form in order to unify the algorithmic framework with approaches in subsequent sections.

2.2 The good

For an insightful understanding of SAM, this subsection focuses on Alg. 1, and establishes convergence for the solver of (1). Assumptions to this end that are common for nonconvex stochastic optimization are listed next [16, 24, 25, 26].

Assumption 1 (lower bounded loss). *Function $f(\mathbf{x})$ is bounded from below, that is, $\exists f^* > -\infty$ such that $f(\mathbf{x}) \geq f^*, \forall \mathbf{x}$.*

Assumption 2 (smoothness). *The stochastic gradient $\mathbf{g}(\mathbf{x})$ is L -Lipschitz, i.e., $\|\mathbf{g}(\mathbf{x}) - \mathbf{g}(\mathbf{y})\| \leq L\|\mathbf{x} - \mathbf{y}\|, \forall \mathbf{x}, \mathbf{y}$.*

Assumption 3 (bounded variance). *The stochastic gradient $\mathbf{g}(\mathbf{x})$ is unbiased with bounded variance, that is, $\mathbb{E}[\mathbf{g}(\mathbf{x})|\mathbf{x}] = \nabla f(\mathbf{x})$ and $\mathbb{E}[\|\mathbf{g}(\mathbf{x}) - \nabla f(\mathbf{x})\|^2|\mathbf{x}] \leq \sigma^2$ for some finite σ .*

Since $\|\epsilon_t\| = \rho$ holds for every t , the pertinent constraint in (1) is never violated; see lines 5 and 6 in Alg. 1. Thus, SAM convergence relates to the behavior of the objective for which a tight result is derived next.

Theorem 1 (SAM convergence). *If Assumptions 1–3 hold, $\eta_t \equiv \eta = \frac{\eta_0}{\sqrt{T}} \leq \frac{2}{3L}$, and $\rho = \frac{\rho_0}{\sqrt{T}}$, then with $c_0 = 1 - \frac{3L\eta}{2} \in (0, 1)$ Alg. 1 guarantees that*

$$\frac{1}{T} \sum_{t=0}^{T-1} \mathbb{E}[\|\nabla f(\mathbf{x}_t)\|^2] = \mathcal{O}\left(\frac{\sigma^2}{\sqrt{T}}\right) \quad \text{and} \\ \frac{1}{T} \sum_{t=0}^{T-1} \mathbb{E}[\|\nabla f(\mathbf{x}_t + \epsilon_t)\|^2] = \mathcal{O}\left(\frac{\sigma^2}{\sqrt{T}}\right).$$

Within a constant factor SAM’s convergence rate is the same as that of SGD; see Appendix D for such a factor included in big \mathcal{O} . Our result avoids the need for a bounded gradient assumption present in prior analyses [16, 26].

A message from Theorem 1 is that *any* adversary satisfying $\epsilon_t \in \mathcal{S}_\rho(\mathbf{0})$ ensures converge. Because the surface $\mathcal{S}_\rho(\mathbf{0})$ is already a huge space, it challenges the plausible optimality of the adversary, and raises a natural question: *Is it possible to find a more powerful adversary to enhance the generalization ability?*

2.3 The challenge: friendly adversary

Adversary to a minibatch can be a friend of other minibatches. SAM’s adversary can be ‘malicious’ for a minibatch \mathcal{B}_t used in iteration t , but not necessarily for other data, because it only safeguards $f_{\mathcal{B}_t}(\mathbf{x}_t + \epsilon_t) - f_{\mathcal{B}_t}(\mathbf{x}_t) \geq 0$ for a small ρ . Given another minibatch data \mathcal{B} , it can be shown that $f_{\mathcal{B}}(\mathbf{x}_t + \epsilon_t) - f_{\mathcal{B}}(\mathbf{x}_t) \leq 0$, whenever the stochastic gradients do not align well, meaning $\langle \mathbf{g}_t(\mathbf{x}_t), \mathbf{g}_{\mathcal{B}}(\mathbf{x}_t) \rangle \leq 0$. Note that such misalignment is common because the variance is massive in large-scale training datasets. This issue will be referred to as *friendly adversary*, and it implies that the adversary vector ϵ_t cannot accurately depict the global sharpness of \mathbf{x}_t . The ‘friendly adversary’ also has a more involved interpretation, that is, $\mathbf{g}_t(\mathbf{x}_t)$ falls outside the column space of Hessian at convergence; see [14, Definition 4.3] for further elaboration. This misalignment of high-order derivatives undermines the inductive bias of SAM, thereby worsening generalization.

To numerically visualize the catastrophic impact of the friendly adversary, we manually introduce one by replacing line 5 of Alg. 1 as $\tilde{\epsilon}_t = \rho \tilde{\mathbf{g}}_t(\mathbf{x}_t) / \|\tilde{\mathbf{g}}_t(\mathbf{x}_t)\|$, where $\tilde{\mathbf{g}}_t$ denotes the gradient on $\tilde{\mathcal{B}}_t$, a randomly sampled batch of the same size as \mathcal{B}_t . This modified approach is denoted as SAM-db, and its performance for i) ResNet-18 on CIFAR10; and, ii) ResNet-34 on

CIFAR100² can be found in Fig. 2(a). Note that the test accuracy is normalized relative to SGD for the ease of visualization. It is evident that the friendly adversary $\tilde{\epsilon}_t$ in SAM-db almost nullifies the generalization benefits entirely.

Source of a friendly adversary. The major cause behind a friendly adversary is due to the gradient variance, which equivalently translates to the lack of stability in SAM’s stochastic linearization (2b). An illustrative three-dimensional example is shown in Fig. 3, where we plot the adversary ϵ_t obtained from different minibatch data. The minibatch gradient is simulated by adding Gaussian noise to the true gradient. When the signal to noise ratio (SNR) is similar to a practical scenario (ResNet-18 on CIFAR10 in Fig. 3 (e)), it can be seen in Fig. 3 (c) and (d) that the adversaries *almost uniformly* spread over the sphere, which strongly indicates how challenging is to evaluate sharpness.

Friendly adversary under the lens of Frank Wolfe. An additional evidence in support of SAM’s friendly adversary resides in its link with stochastic Frank Wolfe (SFW), which also relies heavily on stochastic linearization [27]. The stability of SFW is known to be vulnerable, and its convergence cannot be guaranteed without a sufficiently large batchsize. Appendix A provides the means to obtain friendly adversaries in SAM, and demonstrates that this is tantamount to one-step SFW with a *constant* batchsize. This unveils possible instability of SAM’s stochastic linearization.

2.4 A closer look at friendly adversaries

Gradient variance is a major driver behind SAM’s friendly adversary and unstable stochastic linearization. At first glance however, this seems to conflict with the *empirical* notion of m -sharpness, which asserts that the benefit of SAM is more pronounced when ϵ_t is found using subsampled \mathcal{B}_t of size m , meaning larger variance.

Since m -sharpness hinges heavily on the loss curvature, it is unlikely to hold universally. For example, a transformer is trained on the IWSLT-14 dataset [28], where the test performance (BLEU) decreases with smaller m even if ρ has been tuned carefully; see Fig. 2(c). In principle, m -sharpness is not necessarily related to sharpness or generalization, as verified by the example given in [13, Sec. 3]. Moreover, m -sharpness formulation can be ill-posed for a specific choice of m ; see Appendix B for further details.

Even in the regime where m -sharpness is empirically observed (as with ResNet-18 on CIFAR10 and ResNet-34 on CIFAR100), we have confirmed experimentally that m -sharpness is *not* a consequence of gradient variance; thus, there is contradiction with the friendly adversary pursued in this work.

Observation 1. Same variance, different generalization. Let $m = 128$ and batchsize $b = 128$. Recall the SAM-db experiment in Fig. 2(a). If m -sharpness were a consequence of gradient variance, it would be reasonable to expect that SAM-db has comparable performance to SAM simply because their batchsizes (hence variance) for finding adversaries are the same. Unfortunately, SAM-db exhibits degraded accuracy. We further increase the variance of $\tilde{\mathbf{g}}_t(\mathbf{x}_t)$ by setting $m = 64$. The resultant algorithm is denoted as SAM-db-m/2. It does not catch up with SAM and performs even worse than SAM-db. These experiments validate that variance/stability correlates with the friendly adversary rather than m -sharpness.

Observation 2. Enlarged variance degrades generalization. We explicitly increase variance when finding the adversary by adding Gaussian noise ζ to $\mathbf{g}_t(\mathbf{x}_t)$, i.e., $\tilde{\epsilon}_t = \rho \frac{\mathbf{g}_t(\mathbf{x}_t) + \zeta}{\|\mathbf{g}_t(\mathbf{x}_t) + \zeta\|}$.

2. <https://www.cs.toronto.edu/~kriz/cifar.html>

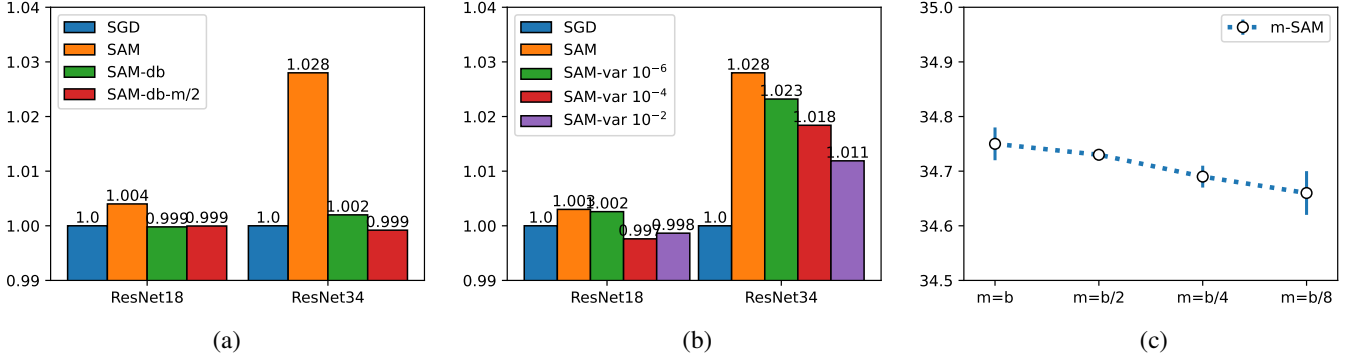


Fig. 2. (a) A friendly adversary diminishes the generalization ability of SAM; (b) m -sharpness may *not* directly correlate with variance since noisy gradient degrades generalization; and (c) m -sharpness may not hold universally. Note that test accuracies in (a) and (b) are normalized to SGD.

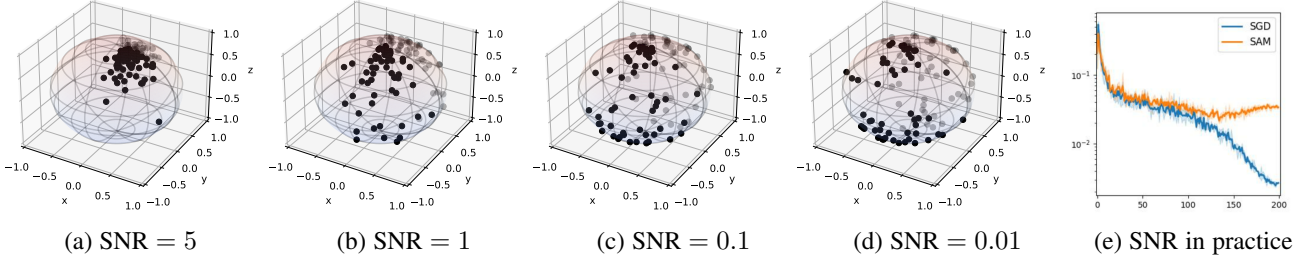


Fig. 3. (a) - (d) SAM's adversaries are spread across the sphere; (e) SNR is in $[0.01, 0.1]$ when training a ResNet-18 on CIFAR10, where the SNR is calculated at the first iteration of every epoch.

After tuning for the best ρ to compensate the variance of ζ , the test performance is plotted in Fig. 2(b). It can be seen that generalization merits clearly decrease with larger variance on both ResNet-18 and ResNet-34. This again illustrates that the plausible benefit of m -sharpness does not stem from increased variance.

While understanding m -sharpness is beyond the scope of this work, Observations 1 and 2 jointly suggest that gradient variance correlates with friendly adversaries rather than m -sharpness.

2.5 The metric: characterization of a friendly adversary

To characterize friendly adversaries analytically, it is convenient to start with necessary notation. Let the *quality* of a stochastic linearization at \mathbf{x}_t with slope \mathbf{v} be $\mathcal{L}_t(\mathbf{v}) := \max_{\|\epsilon\| \leq \rho} f(\mathbf{x}_t) + \langle \mathbf{v}, \epsilon \rangle$. For example, $\mathcal{L}_t(\mathbf{g}_t(\mathbf{x}_t))$ is the quality of SAM. Another critical case is $\mathcal{L}_t(\nabla f(\mathbf{x}_t))$. It is shown in [16] and (2b) that $\mathcal{L}_t(\nabla f(\mathbf{x}_t)) \approx \max_{\|\epsilon\| \leq \rho} f(\mathbf{x}_t + \epsilon)$ when ρ is small. Moreover, $\mathcal{L}_t(\nabla f(\mathbf{x}_t)) - f(\mathbf{x}_t)$ is also an accurate approximation of sharpness. These observations safeguard $\mathcal{L}_t(\nabla f(\mathbf{x}_t))$ as the anchor when analyzing the stability of stochastic linearization.

Definition 1 (δ -stability). A stochastic linearization with slope \mathbf{v} is said to be δ -stable if its quality satisfies $\mathbb{E}[\mathcal{L}_t(\mathbf{v}) - \mathcal{L}_t(\nabla f(\mathbf{x}_t))] \leq \delta$.

Letting $\mathcal{L}_t(\nabla f(\mathbf{x}_t)) - f(\mathbf{x}_t)$ denote ‘sharpness,’ Definition 1 can be decomposed as

$$\begin{aligned} \mathcal{L}_t(\mathbf{v}) - \mathcal{L}_t(\nabla f(\mathbf{x}_t)) &= \underbrace{(\mathcal{L}_t(\mathbf{v}) - f(\mathbf{x}_t))}_{\text{estimated sharpness}} - \underbrace{(\mathcal{L}_t(\nabla f(\mathbf{x}_t)) - f(\mathbf{x}_t))}_{\text{sharpness}}. \end{aligned} \quad (4)$$

The last equation suggests that δ -stability reflects how well sharpness is estimated using slope \mathbf{v} . Hence, a larger δ implies a more friendly adversary, where the sharpness is approximated less

accurately. Next, we will develop our novel approach to ensure improved δ -stability over SAM.

3 VARIANCE SUPPRESSION

This section advocates variance suppression (VASSO) for SAM as a means of dealing with the friendly adversary. We start with the intuition behind VASSO, and then establish its improved δ -stability over SAM. We also develop implementation aspects and possible extensions.

3.1 Design and stability analysis

A straightforward attempt towards stability is to equip SAM's stochastic linearization with variance-reduced gradients such as SVRG and SARAH [29, 30, 31, 32]. However, the requirement to compute a full gradient every few iterations is infeasible, and hardly scales for tasks such as training DNNs.

VASSO overcomes this computational burden through a refined stochastic linearization. For a prescribed $\theta \in (0, 1)$, VASSO is as follows.

$$\text{VASSO: } \mathbf{d}_t = (1 - \theta)\mathbf{d}_{t-1} + \theta \mathbf{g}_t(\mathbf{x}_t) \quad (5a)$$

$$\epsilon_t = \arg \max_{\|\epsilon\| \leq \rho} f(\mathbf{x}_t) + \langle \mathbf{d}_t, \epsilon \rangle = \rho \frac{\mathbf{d}_t}{\|\mathbf{d}_t\|}. \quad (5b)$$

Compared with (2) of SAM, the key difference is that VASSO relies on the slope \mathbf{d}_t in (5b) to promote a more stable stochastic linearization. Slope \mathbf{d}_t is an exponentially moving average (EMA) of $\{\mathbf{g}_t(\mathbf{x}_t)\}_t$ that smooths changes across consecutive iterations. Noticing that ϵ_t and \mathbf{d}_t share the same direction, the relatively smoothed vectors $\{\mathbf{d}_t\}_t$ thus ensure stability of $\{\epsilon_t\}_t$ in VASSO. Moreover, as \mathbf{d}_t processes information of different batches of data, the global sharpness can be captured in a principled manner to alleviate the friendly adversary challenge.

VASSO can be readily integrated with SAM, as summarized in Alg. 1. For convenience, the resultant algorithm is also referred to as VASSO. To theoretically characterize the effectiveness of VASSO, our first result considers \mathbf{d}_t as a qualified strategy to estimate $\nabla f(\mathbf{x}_t)$, and delves into its mean-square error (MSE).

Theorem 2 (Variance suppression). *Under Assumptions 1 – 3, if i) ϵ_t is obtained by (5) with $\theta \in (0, 1)$; and, ii) η_t and ρ are selected as in Theorem 1, then VASSO guarantees that the MSE of \mathbf{d}_t is bounded by*

$$\mathbb{E}[\|\mathbf{d}_t - \nabla f(\mathbf{x}_t)\|^2] \leq \theta\sigma^2 + \mathcal{O}\left(\frac{(1-\theta)^2\sigma^2}{\theta^2\sqrt{T}}\right). \quad (6)$$

Because SAM's gradient estimate has a looser bound on MSE (or variance), that is, $\mathbb{E}[\|\mathbf{g}_t(\mathbf{x}_t) - \nabla f(\mathbf{x}_t)\|^2] \leq \sigma^2$, the shrunk MSE in Theorem 2 justifies the notion of variance suppression.

If we further assume that the gradient is also bounded, meaning $\mathbb{E}[\|\nabla f(\mathbf{x}_t)\|^2] \leq G$, it is possible to further tighten the dependence on T in Theorem 2 as follows

$$\mathbb{E}[\|\mathbf{d}_t - \nabla f(\mathbf{x}_t)\|^2] \leq \theta\sigma^2 + \mathcal{O}\left(\frac{(1-\theta)^2G}{\theta^2T}\right).$$

The proof follows directly by tightening inequality (12) with the bounded gradient assumption. Other theorems in this paper also have an improved T dependence given this extra assumption, but we do not state them explicitly to avoid repetition. Next, we quantify the claimed stability with the suppressed variance.

Theorem 3 (Stabilizing adversaries with VASSO.). *Under Assumptions 1 – 3, and the hyperparameter choices of Theorem 2, the stochastic linearization is $\rho[\sqrt{\theta}\sigma + \mathcal{O}(\frac{\sigma}{\theta T^{1/4}})]$ -stable for VASSO, compared with $\rho\sigma$ -stability of SAM.*

Theorem 3 contends that VASSO alleviates the friendly adversary challenge by promoting stability. Qualitatively, VASSO is roughly $\sqrt{\theta} \in (0, 1)$ times more stable relative to SAM, since the term in big \mathcal{O} notation is negligible given a sufficiently large T . Theorem 3 also guides the choice of θ – preferably small but not too small, otherwise the term in big \mathcal{O} is inversely amplified.

Visualize stabilized adversaries. To validate our findings in Theorem 2, we train a ResNet-18 on CIFAR10 and depict the evolution of $\|\epsilon_t - \epsilon_{t-1}\|$ for both SAM and VASSO in Fig. 4. Because both ϵ_t and ϵ_{t-1} reside on $\mathbb{S}_\rho(\mathbf{0})$, the value of $\|\epsilon_t - \epsilon_{t-1}\|$ is solely determined by the angle between these vectors. In essence, $\|\epsilon_t - \epsilon_{t-1}\|$ characterizes well the stability. The results presented in Fig. 4 distinctly reveal that VASSO indeed improves the stability adversary over SAM.

3.2 Additional perspectives of VASSO

Having dealt with stability, this subsection proceeds with other aspects of VASSO.

Convergence. Summarized in the following corollary, the convergence of VASSO can be pursued as a direct consequence of Theorem 1. The reason is that $\epsilon_t \in \mathbb{S}_\rho(\mathbf{0})$ is satisfied by (5).

Corollary 1 (VASSO convergence). *Under Assumptions 1 – 3, and with η_t and ρ as in Theorem 1, VASSO ensures for any $\theta \in (0, 1)$ that*

$$\frac{1}{T} \sum_{t=0}^{T-1} \mathbb{E}[\|\nabla f(\mathbf{x}_t)\|^2] \leq \mathcal{O}\left(\frac{\sigma^2}{\sqrt{T}}\right) \quad \text{and} \\ \frac{1}{T} \sum_{t=0}^{T-1} \mathbb{E}[\|\nabla f(\mathbf{x}_t + \epsilon_t)\|^2] \leq \mathcal{O}\left(\frac{\sigma^2}{\sqrt{T}}\right).$$

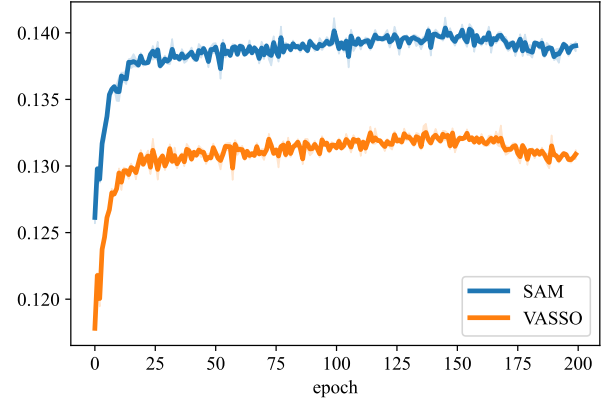


Fig. 4. The adversary of VASSO is more stable than SAM.

Pronounced sharpness around optimum. Consider a near optimal region, where $\|\nabla f(\mathbf{x}_t)\| \rightarrow 0$, and suppose a big data regime, where $\mathbf{g}_t(\mathbf{x}_t) = \nabla f(\mathbf{x}_t) + \zeta$ for some Gaussian random vector ζ with covariance matrix $\sigma^2\mathbf{I}$ for simplicity. (Using arguments from von Mises-Fisher statistics [33] generalization is also possible). SAM has difficulty estimating the flatness in this case, since $\epsilon_t \approx \rho\zeta/\|\zeta\|$ is uniformly distributed over $\mathbb{S}_\rho(\mathbf{0})$ regardless of whether the neighboring region is sharp or not. On the other hand, VASSO has $\epsilon_t = \rho\mathbf{d}_t/\|\mathbf{d}_t\|$. Because $\{\mathbf{g}_\tau(\mathbf{x}_\tau)\}_\tau$ on sharper valleys tend to have larger magnitude, their EMA \mathbf{d}_t is helpful for distinguishing sharp valleys with flat ones.

Memory efficient implementation. Although at first glance VASSO has to store both \mathbf{d}_t and ϵ_t , it can be implemented in a much more memory efficient manner. It is sufficient to store \mathbf{d}_t together with a scalar $\|\mathbf{d}_t\|$ so that ϵ_t can be recovered on demand through normalization; see (5b). Hence, VASSO's memory requirements are the same as those of SAM.

Extensions. VASSO has the potential to boost the performance of other SAM variants by stabilizing their stochastic linearization through variance suppression. For instance, adaptive SAM methods such as [17, 34] are scale invariant, while GSAM [16] minimizes a surrogate gap jointly with (1). Nevertheless, these SAM variants leverage stochastic linearization in (2). It is thus envisioned that VASSO can also alleviate the possible friendly adversary issues therein. As we shall see in Sec. 5, cross-fertilizing VASSO with GSAM yields improved numerical performance.

4 VASSO IMPROVES GENERALIZATION FOR COMPUTATION TRADEOFF

The generalization benefits of SAM come at the price of approximately doubled computation per iteration compared with SGD because of the need to compute $\mathbf{g}_t(\mathbf{x}_t)$ and $\mathbf{g}_t(\mathbf{x}_t + \epsilon_t)$. While there are works trading off generalization for computation [19, 20, 21], unfortunately these efforts are still under the threat of friendly adversaries, suggesting that the optimal tradeoff is elusive.

In pursuit of a more favorable tradeoff that leans toward the generalization side, our idea is to leverage VASSO's stabilized stochastic linearization in eSAM proposed originally in [20]. The resultant algorithm termed as efficient VASSO (eVASSO) is listed as Alg. 2. It introduces a Bernoulli random variable R_t per iteration, where $R_t = 1$ with probability $p \in [0, 1]$. eVASSO alternates between VASSO or SGD based on the value of R_t to save computation. It can be seen that the number of gradient

Algorithm 2 Efficient VASSO (eVASSO)

```

1: Initialize:  $\mathbf{x}_0, \rho, p$ , and a sequence of iid Bernoulli random
   variables  $\{R_t\}_{t=0}^{T-1}$ , where  $R_t = 1$  with probability  $p$ .
2: for  $t = 0, \dots, T-1$  do
3:   Sample a minibatch  $\mathcal{B}_t$ 
4:   Define stochastic gradient on  $\mathcal{B}_t$  as  $\mathbf{g}_t(\cdot)$ 
5:   Calculate  $\mathbf{d}_t = (1 - \theta)\mathbf{d}_{t-1} + \theta\mathbf{g}_t(\mathbf{x}_t)$ 
6:   if  $R_t = 1$  then // Calculate the second gradient
7:      $\epsilon_t = \arg \max_{\|\epsilon\| \leq \rho} f(\mathbf{x}_t) + \langle \mathbf{d}_t, \epsilon \rangle = \rho \frac{\mathbf{d}_t}{\|\mathbf{d}_t\|}$ 
8:     Calculate stochastic gradient  $\hat{\mathbf{g}}_t = \mathbf{g}_t(\mathbf{x}_t + \epsilon_t)$ 
9:   else  $\hat{\mathbf{g}}_t = \mathbf{g}_t(\mathbf{x}_t)$  // Skip gradient computation
10:  end if
11:  Update model via  $\mathbf{x}_{t+1} = \mathbf{x}_t - \eta \hat{\mathbf{g}}_t$ 
12: end for
13: Return:  $\mathbf{x}_T$ 

```

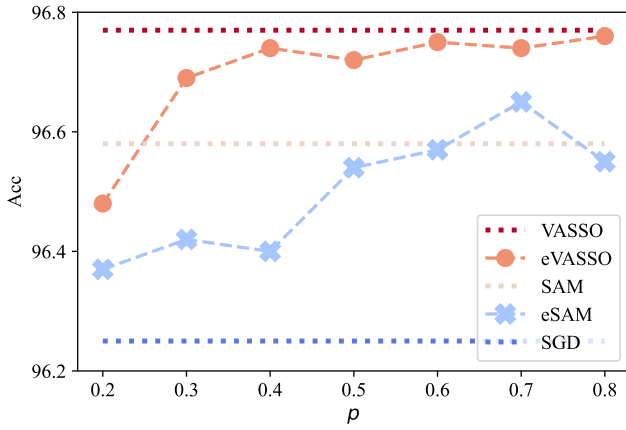


Fig. 5. eVASSO improves generalization-computation tradeoff relative to eSAM.

computation is $(1 + p)$ per iteration in expectation. The hyperparameter p plays a pivotal role in determining the generalization-computation tradeoff of eVASSO. A smaller p advocates more aggressive reduction of computational time, while heightening the risk of compromised generalization comparing with vanilla VASSO. However, thanks to the stabilized stochastic linearization, eVASSO still outperforms SAM for $R_t = 1$, as asserted next.

Theorem 4 (Variance suppression and stability of eVASSO). *Under Assumptions 1 – 3, if i) ϵ_t is obtained by (5) with $\theta \in (0, 1)$; and, ii) η_t and ρ are selected as in Theorem 1, then eVASSO guarantees that for any $p \in (0, 1]$, it holds that*

$$\mathbb{E}[\|\mathbf{d}_t - \nabla f(\mathbf{x}_t)\|^2] \leq \theta\sigma^2 + \mathcal{O}\left(\frac{(1-\theta)^2\sigma^2}{\theta^2\sqrt{T}}\right).$$

Moreover, whenever $R_t = 1$, the stochastic linearization of eVASSO is $\rho[\sqrt{\theta}\sigma + \mathcal{O}(\frac{\sigma}{\theta^{1/4}})]$ -stable.

Note that Theorem 4 is the best one can achieve since there is no need for stochastic linearization when $R_t = 0$.

To visualize the generalization-computation tradeoff in eVASSO relative to eSAM, a ResNet-18 is trained on CIFAR-10 with p chosen from 0.2 to 0.8. The test accuracy is plotted in Fig. 5. It can be seen that eSAM saves computation at the price of compromised test accuracy relative to SAM. However, eVASSO effectively steers the tradeoff towards the desirable side – less computation (small p) with higher accuracy. eVASSO with $p = 0.3$ has already surpassed the performance of vanilla SAM

and eSAM with $p = 0.7$. This means that for the same test accuracy, eVASSO can reduce the computational overhead by 70% and 57% relative to SAM and eSAM, respectively.

5 NUMERICAL TESTS

To support our theoretical findings and validate how powerful variance suppression is, this section assesses generalization performance of VASSO and eVASSO on various learning tasks across vision and language domains. All experiments except those in Sec. 5.2 are run on NVIDIA V100 GPUs. Online code that is used is available at <https://github.com/BingcongLi/VaSSO>.

5.1 Image classification

CIFAR10. Building on the selected base optimizers such as SGD, the test accuracy of VASSO is compared with SAM and two adaptive approaches, namely ASAM and FisherSAM [8, 17, 34]. Neural networks including VGG-11, ResNet-18, WRN-28-10 and PyramidNet-110 are trained on CIFAR10. Standard implementation including random crop, random horizontal flip, normalization and cutout [35] are leveraged for data augmentation. The first three models are trained for 200 epochs with a batchsize of 128, and PyramidNet-110 is trained for 300 epochs using batchsize 256. The cosine learning rate schedule is applied in all settings. The first three models use an initial learning rate of 0.05, and PyramidNet adopts 0.1. Weight decay is chosen as 0.001 for SAM, ASAM, FisherSAM and VASSO, but 0.0005 for SGD following [19, 26]. We tune ρ across the values $\{0.01, 0.05, 0.1, 0.2, 0.5\}$ for SAM; $\rho = 0.1$ yields best results for ResNet and WRN; while $\rho = 0.05$ and $\rho = 0.2$ suit best for VGG and PyramidNet, respectively. ASAM and VASSO adopt the same ρ as SAM. FisherSAM uses the recommended $\rho = 0.1$ [17]. For VASSO, we tune $\theta = \{0.4, 0.9\}$, and report the best accuracy. We find that $\theta = 0.4$ works best for ResNet-18 and WRN-28-10, while $\theta = 0.9$ achieves the best accuracy in other cases.

Table 1 shows that VASSO offers 0.2 to 0.3 accuracy improvement over SAM in all tested scenarios except for PyramidNet-110, where the improvement is about 0.1. These results corroborate that generalizability indeed benefits from variance suppression and the induced stabilized adversary.

CIFAR100. The training setups on this dataset are the same as those on CIFAR10, except that for SAM the best choice is $\rho = 0.2$. The numerical results are listed in Table 2. It can be seen that SAM gains considerably in generalization over SGD, and this gain is further amplified by VASSO. On all tested models, VASSO improves the test accuracy of SAM by 0.2 to 0.3. These experiments once again confirm the improved generalization of VASSO thanks to the stabilized adversary.

ImageNet. Next, we investigate the performance of VASSO on larger scale experiments by training ResNet-50 and ViT-S/32 on ImageNet [36]. Implementation details are deferred to Appendix C. Note that the baseline optimizer is SGD for ResNet and AdamW for ViT [7, 37]. VASSO is also integrated with GSAM (V+G) to demonstrate that variance suppression also benefits other SAM variants such as the one in [16]. For ResNet-50, it can be observed that vanilla VASSO outperforms other SAM variants, and offers a gain of 0.26 over SAM. V+G showcases the best performance with a gain of 0.28 on top of GSAM. VASSO and V+G also exhibit the best test accuracy on ViT-S/32, where VASSO improves SAM by 0.56 and V+G outperforms GSAM by 0.19. These numerical improvement demonstrates that stability of adversaries is indeed desirable.

TABLE 1
Test accuracy (%) of VASSO on various neural networks trained on CIFAR10.

CIFAR10	SGD	SAM	ASAM	FisherSAM	VASSO
VGG-11-BN	93.20 \pm 0.05	93.82 \pm 0.05	93.47 \pm 0.04	93.60 \pm 0.09	94.10 \pm 0.07
ResNet-18	96.25 \pm 0.06	96.58 \pm 0.10	96.33 \pm 0.09	96.72 \pm 0.03	96.77 \pm 0.09
WRN-28-10	97.08 \pm 0.16	97.32 \pm 0.11	97.15 \pm 0.05	97.46 \pm 0.18	97.54 \pm 0.12
PyramidNet-110	97.39 \pm 0.09	97.85 \pm 0.14	97.56 \pm 0.11	97.84 \pm 0.18	97.93 \pm 0.08

TABLE 2
Test accuracy (%) of VASSO on various neural networks trained on CIFAR100.

CIFAR100	SGD	SAM	ASAM	FisherSAM	VASSO
ResNet-18	77.90 \pm 0.07	80.96 \pm 0.12	79.91 \pm 0.04	80.99 \pm 0.13	81.30 \pm 0.13
WRN-28-10	81.71 \pm 0.13	84.88 \pm 0.10	83.54 \pm 0.14	84.91 \pm 0.07	85.06 \pm 0.05
PyramidNet-110	83.50 \pm 0.12	85.60 \pm 0.11	83.72 \pm 0.09	85.55 \pm 0.14	85.85 \pm 0.09

TABLE 3
Test accuracy (%) of VASSO on ImageNet, where V+G is short for VASSO + GSAM.

ImageNet	vanilla	SAM	ASAM	GSAM	VASSO	V+G
ResNet-50	76.62 \pm 0.12	77.16 \pm 0.14	77.10 \pm 0.16	77.20 \pm 0.13	77.42 \pm 0.13	77.48 \pm 0.04
ViT-S/32	68.12 \pm 0.05	68.98 \pm 0.08	68.74 \pm 0.11	69.42 \pm 0.18	69.54 \pm 0.15	69.61 \pm 0.11

TABLE 4
Leave-one-out cross-validation accuracy (%) of VASSO on DomainBed.

DomainBed	Adam	SAM	GSAM	VASSO
PACS	85.5 \pm 0.2	85.8 \pm 0.2	85.9 \pm 0.1	86.0 \pm 0.1
VLCS	77.3 \pm 0.4	79.4 \pm 0.1	79.1 \pm 0.2	79.6 \pm 0.2
OfficeHome	66.5 \pm 0.3	69.6 \pm 0.1	69.3 \pm 0.0	69.8 \pm 0.2
TerraInc	46.1 \pm 1.8	43.3 \pm 0.7	47.0 \pm 0.8	47.0 \pm 0.3
Average	68.9	69.5	70.3	70.6

5.2 Domain generalization

This subsection evaluates VASSO’s efficiency on domain generalization (DG) tasks. The goal of DG is to facilitate seamless transfer of learned knowledge from a “source domain” to generalize well on unseen yet related “target domains” [38, 39]. The major challenge is the distributional shift across these domains, and recent studies have demonstrated that a flat minimum is beneficial to the desirable generalizability [40].

Numerical tests of VASSO are conducted on DomainBed, which is a well-established benchmark [41]. We focus on 4 specific datasets: PACS [42], VLCS [43], OfficeHome [44], and TerraInconita [45]; see Table 9 for details. The performance is

evaluated using standard leave-one-out cross-validation [41], and this experiment is run on a NVIDIA A5000 GPU.

Following [41], a ResNet-50 imported from pytorch and pre-trained on ImageNet is adopted as the backbone. We use a pre-trained checkpoint on purpose – to demonstrate that VASSO can enhance the generalization even for finetuning. Adam is adopted as the base optimizer, and hyperparameters are chosen the same as in [41, 46]. For VASSO, θ takes values from $\{0.2, 0.4, 0.9\}$.

Table 4 compares VASSO with Adam, SAM, and GSAM, where the results of the last three are obtained from [46]. Detailed per-domain results can be found in Appendix C.2. It is observed that VASSO surpasses all these competitors in terms of averaged accuracy, underscoring the benefit of variance suppression in the scenario of distributional shift across diverse domains.

5.3 Label noise

It is known that SAM holds great potential to harness robustness to DNNs under the appearance of label noise in training data [8, 47]. As the training loss landscape is largely perturbed by the label noise, this is a setting where the suppressed variance and stabilized adversaries are expected to improve performance. In our experiments, VASSO’s performance is evaluated when a fraction of the training labels are randomly flipped. With θ taking $\{0.9, 0.4, 0.2\}$ values, the corresponding test accuracies are listed in Table 5.

Our first observation is that VASSO outperforms SAM at all three levels of label noise tested. VASSO elevates generalization

TABLE 5
Test accuracy (%) of VASSO on CIFAR10 under different levels of label noise.

	SAM	VASSO ($\theta = 0.9$)	VASSO ($\theta = 0.4$)	VASSO ($\theta = 0.2$)
25% label noise	96.39 \pm 0.12	96.36 \pm 0.11	96.42 \pm 0.12	96.48 \pm 0.09
50% label noise	93.93 \pm 0.21	94.00 \pm 0.24	94.63 \pm 0.21	94.93 \pm 0.16
75% label noise	75.36 \pm 0.42	77.40 \pm 0.37	80.94 \pm 0.40	85.02 \pm 0.39

TABLE 6
Performance of VASSO for training a Transformer on IWSLT-14 dataset.

	AdamW	SAM	ASAM	VASSO ($\theta = 0.9$)	VASSO ($\theta = 0.4$)
val. ppl.	5.02 \pm 0.03	5.00 \pm 0.04	4.99 \pm 0.03	5.00 \pm 0.03	4.99 \pm 0.03
BLEU	34.66 \pm 0.06	34.75 \pm 0.04	34.76 \pm 0.04	34.81 \pm 0.04	34.88 \pm 0.03

improvement as the percentage of noisy labels grows. For 75% noisy labels, VASSO with $\theta = 0.4$ outperforms SAM with an absolute improvement of 5.58, while VASSO with $\theta = 0.2$ markedly improves SAM by 9.66. In all setups, $\theta = 0.2$ leads to best performance while $\theta = 0.9$ exhibits the worst generalization when compared with VASSO. When fixing the chosen θ , e.g., $\theta = 0.2$, VASSO has larger absolute accuracy improvement over SAM under higher level of label noise. These observations are in agreement with Theorem 3, which predicts that VASSO is suitable for settings with larger label noise due to its enhanced stability, especially when θ is chosen small (but not too small).

5.4 Neural machine translation

Having demonstrated the benefits of variance suppression on vision tasks, here we will test VASSO on German to English translation using a Transformer [28] trained on IWSLT-14 dataset [48], and the fairseq implementation. AdamW is chosen as the base optimizer in SAM and VASSO because of its improved performance over SGD. The learning rate of AdamW is initialized to 5×10^{-4} , and then follows an inverse square root schedule. For momentum, we choose $\beta_1 = 0.9$ and $\beta_2 = 0.98$. Label smoothing is also applied with a rate of 0.1. Hyperparameter ρ is tuned for SAM from $\{0.01, 0.05, 0.1, 0.2\}$, and $\rho = 0.1$ performs the best. The same ρ is picked for ASAM and VASSO.

The validation perplexity and test BLEU scores are listed in Table 6. It can be seen that both SAM and ASAM have better performance on validation perplexity and BLEU relative to AdamW. Although VASSO with $\theta = 0.9$ has slightly higher validation perplexity, its BLEU score outperforms SAM and ASAM. VASSO with $\theta = 0.4$ showcases the best generalization performance on this task, providing a 0.22 improvement on BLEU score relative to AdamW. This aligns with Theorems 2 and 3, which suggest that a small θ is more beneficial to the stability of adversaries.

5.5 Generalization-computation tradeoff

As previously illustrated in Fig. 5, eVASSO improves the generalization-computation tradeoff. This subsection offers fur-

ther supporting evidence to this end. In particular, the proposed eVASSO with $p = 0.5$ and $p = 0.3$ is tested on ResNet-18 and WRN-28-10 using datasets CIFAR10 and CIFAR100. The test accuracy vs runtime of eVASSO, and benchmark algorithms such as SGD, SAM and eSAM can be found in Table 7. Note that for eVASSO, we tune θ from $\{0.4, 0.9\}$, and report the best results.

As expected, the excess runtime of eVASSO and eSAM relative to SGD is roughly proportional to p . Another common observation is that a smaller p degrades generalization, demonstrating the tradeoff pattern.

CIFAR10. Compared with SAM, eVASSO achieves better and comparable test accuracy on ResNet-18 and WRN-28-10, respectively, while requiring significantly reduced training time. On the other hand, eVASSO utilizes similar computational resources to reach markedly improved test accuracy over eSAM, because of the suppressed variance for finding adversaries.

CIFAR100. On ResNet-18, the test accuracy of eVASSO with $p = 0.5$ outperforms SAM, and with $p = 0.3$ it is comparable to SAM. While on WRN-28-10, although eVASSO cannot match with SAM, it significantly outperforms eSAM and SGD. This suggests that even with minimally increased computation time (e.g., 1.3x), it is possible to improve the generalization over SGD drastically by 2.3.

5.6 Additional tests

This subsection evaluates several flatness-related metrics using a ResNet-18 trained on CIFAR10, where the hyperparameters are chosen as those in Sections 5.1 and 5.5.

Hessian spectrum. We focus on the largest eigenvalue λ_1 and the ratio of the largest to the fifth largest eigenvalue λ_1/λ_5 . These metrics are also adopted by [8, 49] to reflect the flatness of the solution, where smaller numbers are more preferable. Because exact calculation of the Hessian spectrum is prohibitive given the ResNet-18 size, we instead leverage Lanczos' approximation algorithm [50]. Table 8 shows that SAM indeed converges to a much flatter solution compared with SGD, and VASSO further

TABLE 7

Test accuracy and epoch runtime of eVASSO on CIFAR-10 and CIFAR-100 datasets. The numbers in parentheses (·) indicate the ratio of training speed relative to SGD.

	ResNet-18		WRN-28-10	
CIFAR-10	Accuracy	epoch runtime (s)	Accuracy	epoch runtime (s)
SGD	96.25 \pm 0.05	14.42 (1x)	97.08 \pm 0.16	80.58 (1x)
SAM	96.58 \pm 0.10	27.62 (1.92x)	97.32 \pm 0.11	156.92 (1.95x)
eSAM ($p = 0.5$)	96.54 \pm 0.11	21.57 (1.49x)	97.21 \pm 0.08	119.06 (1.48x)
eVASSO ($p = 0.5$)	96.72 \pm 0.14	21.94 (1.52x)	97.36 \pm 0.11	120.11 (1.49x)
eSAM ($p = 0.3$)	96.42 \pm 0.08	18.34 (1.27x)	97.20 \pm 0.11	105.63 (1.31x)
eVASSO ($p = 0.3$)	96.69 \pm 0.06	18.61 ((1.29x)	97.29 \pm 0.16	105.99 (1.32x)
CIFAR-100	Accuracy	epoch runtime (s)	Accuracy	epoch runtime (s)
SGD	77.90 \pm 0.07	14.87 (1x)	81.71 \pm 0.13	81.02 (1x)
SAM	80.96 \pm 0.12	28.37 (1.91x)	84.88 \pm 0.10	157.44 (1.94x)
eSAM ($p = 0.5$)	81.03 \pm 0.17	21.77 (1.46x)	84.31 \pm 0.15	120.28 (1.48x)
eVASSO ($p = 0.5$)	81.20 \pm 0.15	22.09 (1.49x)	84.52 \pm 0.06	121.55 (1.49x)
eSAM ($p = 0.3$)	80.60 \pm 0.12	19.32 (1.30x)	83.65 \pm 0.18	105.41 (1.30x)
eVASSO ($p = 0.3$)	80.84 \pm 0.06	19.35 ((1.30x)	84.07 \pm 0.08	106.61 (1.30x)

TABLE 8
Hessian spectrum of a ResNet-18.

	SGD	SAM	VASSO	eVASSO
λ_1	82.52	26.40	23.32	25.21
λ_1/λ_5	16.63	2.12	1.86	2.03

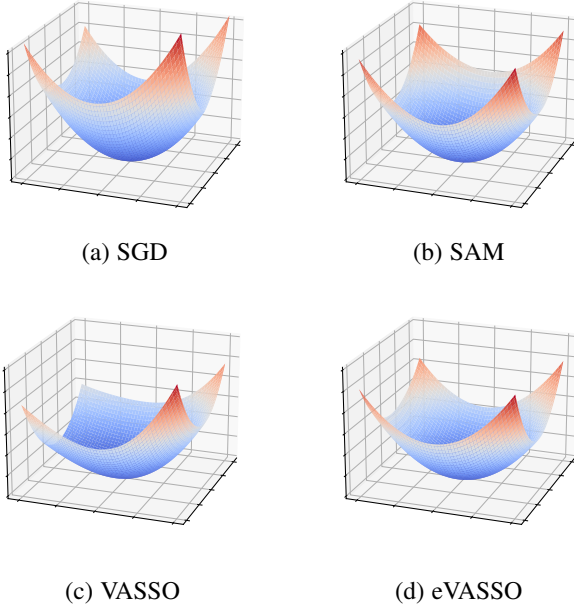


Fig. 6. Visualization of loss landscapes.

improves upon SAM. This confirms that the friendly adversary effect is indeed alleviated by variance suppression, which in turn boosts the generalization of ResNet18 as shown earlier in Section 5.1. Moreover, the flatness measure of eVASSO with $p = 0.5$ is slightly worse compared with VASSO. This is a consequence of the computation-generalization tradeoff that is present in eVASSO.

Landscape. The loss landscapes optimized by the proposed approaches are plotted in Fig. 6 following the visualization method in [51]. It can be seen that VASSO and eVASSO ($p = 0.5$) indeed

find flatter valleys relative to SAM and SGD, in agreement with their improved generalization behavior.

6 OTHER RELATED WORKS

This section completes the context of DNN generalizability with related works.

Sharpness and generalization. Since the study of [10], the relation between sharpness and generalization has been investigated intensively. It has been observed that sharpness is closely correlated with the ratio between learning rate and batchsize in SGD [52]. Analytical results on the generalization error using sharpness-related measures can be found in e.g., [53, 54, 55]. These works justify the goal of seeking a flatter valley to enhance generalizability. Aiming at a flatter minimum, approaches other than SAM have been also developed. For example, stochastic weight averaging has been advocated for DNNs [56], while [57] has put forth an algorithm similar to SAM and has placed emphasis on robustness to adversarial training.

SAM variants. Besides GSAM and ASAM that have been already mentioned, [58] pursued a SAM variant by penalizing the gradient norm on the premise that sharper valleys tend to have gradients with larger norm. In addition, [59] arrived at a similar conclusion by analyzing gradient flow. Exploiting

multiple (ascent) steps to find an adversary has been studied systematically [60]. However, these works overlook the friendly adversary issue, while VASSO provides algorithmic possibilities for generalization benefits by stabilizing their adversaries.

7 CONCLUDING REMARKS

This contribution demonstrates that stabilizing adversaries through variance suppression consolidates the generalization merits of sharpness-aware minimization. The novel framework abbreviated as VASSO, induces provable stability for SAM's stochastic linearization. VASSO's theoretically established merits are demonstrated with a suit of numerical experiments, and illustrate model-agnostic improvement over SAM on various vision and language tasks. Lastly, VASSO also steers the generalization-computation tradeoff of SAM towards the optimal side – improved generalization (over SGD) with significantly reduced computation (relative to SAM).

REFERENCES

- [1] J. Devlin, M.-W. Chang, K. Lee, and K. Toutanova, “Bert: Pre-training of deep bidirectional transformers for language understanding,” *arXiv:1810.04805*, 2018.
- [2] B. Tom, M. Benjamin, R. Nick, S. Melanie, K. Jared, D. Prafulla, N. Arvind, S. Pranav, S. Girish, A. Amanda, A. Sandhini, H.-V. Ariel, K. Gretchen, H. Tom, C. Rewon, R. Aditya, Z. D. M., W. Jeffrey, W. Clemens, H. Christopher, C. Mark, S. Eric, L. Mateusz, G. Scott, C. Benjamin, C. Jack, B. Christopher, M. Sam, R. Alec, S. Ilya, and A. Dario, “Language models are few-shot learners,” in *Proc. Adv. Neural Info. Processing Systems*, vol. 33, 2020, pp. 1877–1901.
- [3] C. Zhang, S. Bengio, M. Hardt, B. Recht, and O. Vinyals, “Understanding deep learning (still) requires rethinking generalization,” *Communications of the ACM*, vol. 64, no. 3, pp. 107–115, 2021.
- [4] N. Srivastava, G. E. Hinton, A. Krizhevsky, I. Sutskever, and R. Salakhutdinov, “Dropout: a simple way to prevent neural networks from overfitting,” *J. Mach. Learn. Res.*, vol. 15, pp. 1929–1958, 2014.
- [5] X. Chen, C.-J. Hsieh, and B. Gong, “When vision transformers outperform resnets without pre-training or strong data augmentations,” in *Proc. Int. Conf. Learning Representation*, 2022.
- [6] A. C. Wilson, R. Roelofs, M. Stern, N. Srebro, B. Recht, and N. Srebro, “The marginal value of adaptive gradient methods in machine learning,” in *Proc. Int. Conf. Machine Learning*, vol. 30, 2017, pp. 4148–4158.
- [7] I. Loshchilov and F. Hutter, “Decoupled weight decay regularization,” in *Proc. Int. Conf. Learning Representation*, 2017.
- [8] P. Foret, A. Kleiner, H. Mobahi, and B. Neyshabur, “Sharpness-aware minimization for efficiently improving generalization,” in *Proc. Int. Conf. Learning Representation*, 2021.
- [9] Y. Jiang, B. Neyshabur, D. Krishnan, H. Mobahi, and S. Bengio, “Fantastic generalization measures and where to find them,” *arXiv:1912.02178*, 2019.
- [10] N. S. Keskar, D. Mudigere, J. Nocedal, M. Smelyanskiy, and P. T. P. Tang, “On large-batch training for deep learning: Generalization gap and sharp minima,” in *Proc. Int. Conf. Learning Representation*, 2016.
- [11] P. Chaudhari, A. Choromanska, S. Soatto, Y. LeCun, C. Baldassi, C. Borgs, J. Chayes, L. Sagun, and R. Zecchina, “Entropy-SGD: Biasing gradient descent into wide valleys,” in *Proc. Int. Conf. Learning Representation*, 2017.
- [12] Z. Zhang, R. Luo, Q. Su, and X. Sun, “GA-SAM: Gradient-strength based adaptive sharpness-aware minimization for improved generalization,” in *Proc. Conf. Empirical Methods in Natural Language Processing*, 2022.
- [13] M. Andriushchenko and N. Flammarion, “Towards understanding sharpness-aware minimization,” in *Proc. Int. Conf. Machine Learning*, 2022, pp. 639–668.
- [14] K. Wen, T. Ma, and Z. Hiyuan Li, “How does sharpness-aware minimization minimizes sharpness,” in *Proc. Int. Conf. Learning Representation*, 2023.
- [15] P. L. Bartlett, P. M. Long, and O. Bousquet, “The dynamics of sharpness-aware minimization: Bouncing across ravines and drifting towards wide minima,” *arXiv:2210.01513*, 2022.
- [16] J. Zhuang, B. Gong, L. Yuan, Y. Cui, H. Adam, N. Dvornek, S. Tatikonda, J. Duncan, and T. Liu, “Surrogate gap minimization improves sharpness-aware training,” in *Proc. Int. Conf. Learning Representation*, 2022.
- [17] M. Kim, D. Li, S. X. Hu, and T. M. Hospedales, “Fisher SAM: Information geometry and sharpness aware minimization,” in *Proc. Int. Conf. Machine Learning*, 2022, pp. 11 148–11 161.
- [18] Y. Liu, S. Mai, X. Chen, C.-J. Hsieh, and Y. You, “Towards efficient and scalable sharpness-aware minimization,” in *Proc. Conf. Computer Vision and Pattern Recognition*, vol. 2022, 2022, pp. 12 350–12 360.
- [19] J. Du, H. Yan, J. Feng, J. T. Zhou, L. Zhen, R. S. M. Goh, and V. Y. F. Tan, “Efficient sharpness-aware minimization for improved training of neural networks,” in *Proc. Int. Conf. Learning Representation*, 2022.
- [20] Y. Zhao, H. Zhang, and X. Hu, “SS-SAM: Stochastic scheduled sharpness-aware minimization for efficiently training deep neural networks,” *arXiv:2203.09962*, 2022.
- [21] W. Jiang, H. Yang, Y. Zhang, and J. Kwok, “An adaptive policy to employ sharpness-aware minimization,” *arXiv:2304.14647*, 2023.
- [22] J. Du, D. Zhou, J. Feng, V. Y. F. Tan, and J. T. Zhou, “Sharpness-aware training for free,” in *Proc. Adv. Neural Info. Processing Systems*, 2022.
- [23] B. Li and G. B. Giannakis, “Enhancing sharpness-aware optimization through variance suppression,” in *Proc. Adv. Neural Info. Processing Systems*, 2023.
- [24] S. Ghadimi and G. Lan, “Stochastic first-and zeroth-order methods for nonconvex stochastic programming,” *SIAM Journal on Optimization*, vol. 23, no. 4, pp. 2341–2368, 2013.
- [25] L. Bottou, F. E. Curtis, and J. Nocedal, “Optimization methods for large-scale machine learning,” *arXiv preprint arXiv:1606.04838*, 2016.
- [26] P. Mi, L. Shen, T. Ren, Y. Zhou, X. Sun, R. Ji, and D. Tao, “Make sharpness-aware minimization stronger: A sparsified perturbation approach,” in *Proc. Adv. Neural Info. Processing Systems*, 2022.
- [27] S. J. Reddi, S. Sra, B. Póczos, and A. Smola, “Stochastic Frank-Wolfe methods for nonconvex optimization,” in *Allerton conference on communication, control, and computing*. IEEE, 2016, pp. 1244–1251.
- [28] A. Vaswani, N. Shazeer, N. Parmar, J. Uszkoreit, L. Jones,

- A. N. Gomez, Ł. Kaiser, and I. Polosukhin, "Attention is all you need," in *Proc. Adv. Neural Info. Processing Systems*, vol. 30, 2017.
- [29] R. Johnson and T. Zhang, "Accelerating stochastic gradient descent using predictive variance reduction," in *Proc. Advances in Neural Info. Process. Syst.*, Lake Tahoe, Nevada, 2013, pp. 315–323.
- [30] L. M. Nguyen, J. Liu, K. Scheinberg, and M. Takáč, "SARAH: A novel method for machine learning problems using stochastic recursive gradient," in *Proc. Int. Conf. Machine Learning*, Sydney, Australia, 2017.
- [31] B. Li, L. Wang, and G. B. Giannakis, "Almost tune-free variance reduction," in *Proc. Intl. Conf. on Machine Learning*, 2020.
- [32] B. Li, M. Ma, and G. B. Giannakis, "On the convergence of SARAH and beyond," in *Proc. Int. Conf. Artif. Intel. and Stats.*, 2019.
- [33] K. V. Mardia and P. E. Jupp, *Directional Statistics*. Directional statistics, 2000.
- [34] J. Kwon, J. Kim, H. Park, and I. K. Choi, "ASAM: Adaptive sharpness-aware minimization for scale-invariant learning of deep neural networks," in *Proc. Int. Conf. Machine Learning*, vol. 139, 2021, pp. 5905–5914.
- [35] T. Devries and G. W. Taylor, "Improved regularization of convolutional neural networks with cutout," vol. abs/1708.04552, 2017.
- [36] J. Deng, W. Dong, R. Socher, L.-J. Li, K. Li, and L. Fei-Fei, "ImageNet: A large-scale hierarchical image database," in *Proc. Conf. Computer Vision and Pattern Recognition*, 2009, pp. 248–255.
- [37] D. P. Kingma and J. Ba, "Adam: A method for stochastic optimization," in *Proc. Int. Conf. Learning Representation*, 2014.
- [38] K. Zhou, Z. Liu, Y. Qiao, T. Xiang, and C. C. Loy, "Domain generalization: A survey," *IEEE Trans. Pattern Analysis and Machine Intelligence*, 2022.
- [39] P. Oza, V. A. Sindagi, V. V. Sharmini, and V. M. Patel, "Unsupervised domain adaptation of object detectors: A survey," *IEEE Trans. Pattern Analysis and Machine Intelligence*, 2023.
- [40] P. Wang, Z. Zhang, Z. Lei, and L. Zhang, "Sharpness-aware gradient matching for domain generalization," in *Proc. Conf. Computer Vision and Pattern Recognition*, 2023, pp. 3769–3778.
- [41] I. Gulrajani and D. Lopez-Paz, "In search of lost domain generalization," in *Proc. Int. Conf. Learning Representation*, 2020.
- [42] D. Li, Y. Yang, Y.-Z. Song, and T. M. Hospedales, "Deeper, broader and artier domain generalization," Oct 2017.
- [43] C. Fang, Y. Xu, and D. N. Rockmore, "Unbiased metric learning: On the utilization of multiple datasets and web images for softening bias," December 2013.
- [44] H. Venkateswara, J. Eusebio, S. Chakraborty, and S. Panchanathan, "Deep hashing network for unsupervised domain adaptation," in *Proc. Conf. Computer Vision and Pattern Recognition*, July 2017.
- [45] S. Beery, G. Van Horn, and P. Perona, "Recognition in terra incognita," September 2018.
- [46] P. Wang, Z. Zhang, Z. Lei, and L. Zhang, "Sharpness-aware gradient matching for domain generalization," in *Proc. Conf. Computer Vision and Pattern Recognition*, June 2023, pp. 3769–3778.
- [47] S. Jiang, J. Li, J. Zhang, Y. Wang, and T. Xu, "Dynamic loss for robust learning," *IEEE Trans. Pattern Analysis and Machine Intelligence*, 2023.
- [48] M. Cettolo, J. Niehues, S. Stker, L. Bentivogli, and M. Federico, "Report on the 11th iwslt evaluation campaign, iwslt 2014," 2014.
- [49] S. Jastrzebski, M. Szymczak, S. Fort, D. Arpit, J. Tabor, K. Cho, and K. J. Geras, "The break-even point on optimization trajectories of deep neural networks," in *Proc. Int. Conf. Learning Representation*, 2020.
- [50] B. Ghorbani, S. Krishnan, and Y. Xiao, "An investigation into neural net optimization via hessian eigenvalue density," in *Proc. Int. Conf. Machine Learning*, 2019, pp. 2232–2241.
- [51] H. Li, Z. Xu, G. Taylor, C. Studer, and T. Goldstein, "Visualizing the loss landscape of neural nets," vol. 31, 2018.
- [52] S. Jastrzebski, Z. Kenton, D. Arpit, N. Ballas, A. Fischer, Y. Bengio, and A. Storkey, "Three factors influencing minima in sgd," *arXiv:1711.04623*, 2017.
- [53] G. K. Dziugaite and D. M. Roy, "Computing nonvacuous generalization bounds for deep (stochastic) neural networks with many more parameters than training data," in *Proc. Conf. Uncertainty in Artif. Intel.*, 2017.
- [54] B. Neyshabur, S. Bhojanapalli, D. Mcallester, N. Srebro, and N. Srebro, "Exploring generalization in deep learning," in *Proc. Adv. Neural Info. Processing Systems*, vol. 30, 2017, pp. 5947–5956.
- [55] Z. Wang and Y. Mao, "On the generalization of models trained with sgd: Information-theoretic bounds and implications," in *Proc. Int. Conf. Learning Representation*, 2022.
- [56] P. Izmailov, D. Podoprikin, T. Garipov, D. P. Vetrov, and A. G. Wilson, "Averaging weights leads to wider optima and better generalization," in *Proc. Conf. Uncertainty in Artif. Intel.*, 2018, pp. 876–885.
- [57] D. Wu, S.-T. Xia, and Y. Wang, "Adversarial weight perturbation helps robust generalization," in *Proc. Adv. Neural Info. Processing Systems*, vol. 33, 2020, pp. 2958–2969.
- [58] Y. Zhao, H. Zhang, and X. Hu, "Penalizing gradient norm for efficiently improving generalization in deep learning," in *Proc. Int. Conf. Machine Learning*, 2022, pp. 26 982–26 992.
- [59] D. G. Barrett and B. Dherin, "Implicit gradient regularization," in *Proc. Int. Conf. Learning Representation*, 2021.
- [60] H. Kim, J. Park, Y. Choi, W. Lee, and J. Lee, "Exploring the effect of multi-step ascent in sharpness-aware minimization," *arXiv:2302.10181*, 2023.
- [61] A. Mokhtari, H. Hassani, and A. Karbasi, "Stochastic conditional gradient methods: From convex minimization to submodular maximization," *Journal of Machine Learning Research*, vol. 21, no. 1, pp. 4232–4280, 2020.
- [62] Y. Zhang, B. Li, and G. B. Giannakis, "Accelerating Frank-Wolfe with weighted average gradients," in *Proc. IEEE Int. Conf. Acoust., Speech, Sig. Process.*, 2021, pp. 5529–5533.
- [63] B. Li, A. Sadeghi, and G. Giannakis, "Heavy ball momentum for conditional gradient," in *Proc. Advances in Neural Info. Process. Syst.*, 2021.
- [64] T. Tsiligkaridis and J. Roberts, "Understanding and increasing efficiency of Frank-Wolfe adversarial training," in *Proc. Conf. Computer Vision and Pattern Recognition*, 2022, pp. 50–59.
- [65] B. Li, M. Coutino, G. B. Giannakis, and G. Leus, "A momentum-guided Frank-Wolfe algorithm," *IEEE Trans. on*

Signal Processing, vol. 69, pp. 3597–3611, 2021.

- [66] B. Li, L. Wang, G. B. Giannakis, and Z. Zhao, “Enhancing Frank-Wolfe with an extra subproblem,” in *Proc. of 35th AAAI Conf. on Artificial Intelligence*, 2021.
- [67] F. Huang, L. Tao, and S. Chen, “Accelerated stochastic gradient-free and projection-free methods,” in *Proc. Int. Conf. Machine Learning*. PMLR, 2020, pp. 4519–4530.

APPENDIX A

SFW VIS-A-VIS SAM ADVERSARY

The stochastic Frank-Wolfe (SFW) algorithm outlined in Alg. 3 solves the following generally nonconvex stochastic optimization

$$\max_{\mathbf{x} \in \mathcal{X}} h(\mathbf{x}) := \mathbb{E}_{\xi} [h(\mathbf{x}, \xi)] \quad (7)$$

where \mathcal{X} is a convex and compact constraint set.

Algorithm 3 SFW [27]

```

1: Initialize:  $\mathbf{x}_0 \in \mathcal{X}$ 
2: for  $t = 0, 1, \dots, T - 1$  do
3:   draw iid samples  $\{\xi_t^b\}_{b=1}^{B_t}$ 
4:   let  $\hat{\mathbf{g}}_t = \frac{1}{B_t} \sum_{b=1}^{B_t} \nabla h(\mathbf{x}_t, \xi_t^b)$ 
5:    $\mathbf{v}_{t+1} = \arg \max_{\mathbf{v} \in \mathcal{X}} \langle \hat{\mathbf{g}}_t, \mathbf{v} \rangle$ 
6:    $\mathbf{x}_{t+1} = (1 - \gamma_t) \mathbf{x}_t + \gamma_t \mathbf{v}_{t+1}$ 
7: end for
```

The SFW iteration is convergent so long as the batchsize $B_t = \mathcal{O}(T)$, $\forall t$ is sufficiently large [27, Theorem 2]. This is because line 5 in Alg. 3 is extremely sensitive to gradient noise.

A.1 The adversary of SAM

By choosing $h(\epsilon) = f(\mathbf{x}_t + \epsilon)$ and $\mathcal{X} = \mathbb{S}_\rho(\mathbf{0})$, it is not hard to show that 1-iteration SFW with $\gamma_0 = 1$ yields a solution equivalent to the stochastic linearization in SAM; cf. (2) and (3). This link implies that the SAM adversary also suffers from stability issues in the same way as SFW does. Moreover, what amplifies this issue in SAM is the adoption of a constant batchsize, which is typically small and far less than the $\mathcal{O}(T)$ required for SFW convergence.

Our VASSO solver is inspired by modified SFW approaches that leverage a constant batchsize to ensure convergence; see e.g., [61, 62, 63]. Even though, coping with SAM’s instability is still challenging in two major aspects. First, SAM uses *one-step* SFW, which internally breaks the nice analytical structure. Moreover, the inner maximization (i.e., the objective function of SFW) *varies from iteration to iteration* along with the updated \mathbf{x}_t . This link also suggests the potential of applying other FW approaches for the adversary such as those in [64, 65, 66, 67]. We leave this direction for future research.

A.2 The three dimensional example in Fig. 3

Here we detail the implementation used for generating Fig. 3. We use $\nabla f(\mathbf{x}) = [0.2, -0.1, 0.6]$, and stochastic noise $\xi = [\xi_1, \xi_2, \xi_3]$, where ξ_1, ξ_2, ξ_3 are iid Gaussian random variables with variance scaling with 0.2, 1, 2, respectively. Scaling is used to vary the SNR. We generate 100 adversaries by solving $\arg \max_{\|\epsilon\| \leq \rho} \langle \nabla f(\mathbf{x}) + \xi, \epsilon \rangle$ for each SNR value. As shown in Fig. 3, the adversaries are unlikely to capture the sharpness information when the SNR is small, because they spread indistinguishably all over the sphere.

TABLE 9
Summary of DomainBed benchmark

dataset	# images	# classes
PACS	9,991	7
VLCS	10,729	5
OfficeHome	15,588	65
TerraInc	24,788	10

APPENDIX B

MORE ON m -SHARPNESS

m -sharpness can be ill-posed. Our reason for not studying m -sharpness directly is that its formulation [13, eq. (3)] may be ill-posed mathematically due to the lack of a clear definition on how the dataset \mathcal{S} is partitioned. Consider the following example, where the same notation as [13] is adopted for convenience. Suppose that the loss function is $l_i(w) = a_i w^2 + b_i w$, where $\{(a_i, b_i)\}_i$ are data points, and w is the parameter to be optimized. Let the dataset have 4 samples, $(a_1 = 0, b_1 = 1)$; $(a_2 = 0, b_2 = -1)$; $(a_3 = -1, b_3 = 0)$; and, $(a_4 = 1, b_4 = 0)$. Consider 2-sharpness.

- If the data partition is $\{1,2\}$ and $\{3,4\}$, the objective of 2-sharpness, namely equation (3) in [13], becomes $\min_w \sum_{i=1}^2 \max_{\|\delta\| < \rho} 0$.
- If the data partition is $\{1,3\}$ and $\{2,4\}$, the objective is $\min_w \sum_{i=1}^2 \max_{\|\delta\| < \rho} f_i(w, \delta)$, where f_1 is the loss on partition $\{1,3\}$, that is, $f_1(w, \delta) = -(w + \delta)^2 + (w + \delta)$; and $f_2(w, \delta) = (w + \delta)^2 - (w + \delta)$ is the loss on partition $\{3,4\}$.

The objective functions are different when the data partition varies. This makes the problem ill-posed – data partition leads to entirely different loss curvature. In practice, the data partition even varies across epochs due to the random shuffle in data loading.

APPENDIX C

DETAILS ON NUMERICAL TESTS

C.1 ImageNet

ResNet50. Due to limitations of computational resources, we report the averaged results over 2 independent runs. For this dataset, we randomly resize and crop all images to a resolution of 224×224 , and apply random horizontal flip, as well as normalization during training. The batchsize is 128 with a cosine learning rate scheduling and with initial step size 0.05. The momentum and weight decay of the base optimizer, here SGD, are set to 0.9 and 10^{-4} , respectively. We tune ρ from $\{0.05, 0.075, 0.1, 0.2\}$, and choose $\rho = 0.075$ for SAM. VASSO uses $\theta = 0.99$. VASSO and ASAM adopt the same $\rho = 0.075$.

ViT-S/32. We follow the implementation of [22], where we train the model for 300 epochs with a batchsize of 4096. The baseline optimizer is chosen as AdamW with weight decay 0.3. SAM relies on $\rho = 0.05$. For the implementation of GSAM and V+G, we adopt the same implementation from [16].

C.2 Domain generalization

Table 9 includes details of the DomainBed benchmark [41]; while Tables 10, 11, 12, and 13 provide leave-one-out cross-validation results per dataset.

TABLE 10
Cross-validation accuracies (%) on PACS dataset.

Test domain	Adam	SAM	GSAM	VASSO
Photo	97.2 \pm 0.3	97.0 \pm 0.4	97.5 \pm 0.0	95.4 \pm 0.2
Art painting	84.7 \pm 0.4	85.6 \pm 2.1	86.9 \pm 0.1	84.2 \pm 0.6
Cartoon	80.8 \pm 0.6	80.9 \pm 1.2	80.4 \pm 0.2	81.8 \pm 0.5
Sketch	79.3 \pm 1.0	79.6 \pm 1.6	78.7 \pm 0.8	82.5 \pm 0.4
Average	85.5	85.8	85.9	86.0

TABLE 11
Cross-validation accuracies (%) on VLCS dataset.

Test domain	Adam	SAM	GSAM	VASSO
VOC2007	75.2 \pm 1.6	79.8 \pm 0.1	78.5 \pm 0.8	78.9 \pm 0.7
LabelMe	64.7 \pm 1.2	65.0 \pm 1.0	64.9 \pm 0.2	65.9 \pm 0.5
Caltech101	98.0 \pm 0.3	99.1 \pm 0.2	98.7 \pm 0.3	99.0 \pm 0.2
SUN09	71.4 \pm 1.2	73.7 \pm 1.0	74.3 \pm 0.0	74.4 \pm 0.9
Average	77.3	79.4	79.1	79.6

TABLE 12
Cross-validation accuracies (%) on OfficeHome dataset.

Test domain	Adam	SAM	GSAM	VASSO
Art	61.3 \pm 0.7	64.5 \pm 0.3	64.9 \pm 0.1	64.8 \pm 0.5
Clipart	52.4 \pm 0.3	56.5 \pm 0.2	55.2 \pm 0.2	57.1 \pm 0.4
Product	75.8 \pm 0.1	77.4 \pm 0.1	77.8 \pm 0.0	78.2 \pm 0.2
Real world	76.6 \pm 0.3	79.8 \pm 0.4	79.2 \pm 0.2	79.3 \pm 0.1
Average	66.5	69.6	69.3	69.8

TABLE 13
Cross-validation accuracies (%) on TerraIncognita dataset.

Test domain	Adam	SAM	GSAM	VASSO
Location 38	42.1 \pm 1.4	38.4 \pm 2.4	39.3 \pm 0.2	38.5 \pm 0.7
Location 43	56.9 \pm 1.8	54.0 \pm 1.0	59.6 \pm 0.0	60.7 \pm 0.2
Location 46	35.7 \pm 3.9	34.5 \pm 0.8	38.2 \pm 0.8	37.5 \pm 0.8
Location 100	49.8 \pm 4.4	46.3 \pm 1.0	50.8 \pm 0.1	51.4 \pm 0.8
Average	46.1	43.3	47.0	47.0

APPENDIX D MISSING PROOFS

Alg. 1 can be written as

$$\mathbf{x}_{t+\frac{1}{2}} = \mathbf{x}_t + \epsilon_t \quad (8a)$$

$$\mathbf{x}_{t+1} = \mathbf{x}_t - \eta_t \mathbf{g}_t(\mathbf{x}_{t+\frac{1}{2}}) \quad (8b)$$

where $\|\epsilon_t\| = \rho$. In SAM, we have $\epsilon_t = \rho \frac{\mathbf{g}_t(\mathbf{x}_t)}{\|\mathbf{g}_t(\mathbf{x}_t)\|}$, and in VASSO we have $\epsilon_t = \rho \frac{\mathbf{d}_t}{\|\mathbf{d}_t\|}$.

D.1 Useful lemmas

This subsection presents useful lemmas for our main results.

Lemma 1. Alg. 1 (or equivalently iteration (8)) ensures that

$$\begin{aligned} \eta_t \mathbb{E}[\langle \nabla f(\mathbf{x}_t), \nabla f(\mathbf{x}_t) - \mathbf{g}_t(\mathbf{x}_{t+\frac{1}{2}}) \rangle] \\ \leq \frac{L\eta_t^2}{2} \mathbb{E}[\|\nabla f(\mathbf{x}_t)\|^2] + \frac{L\rho^2}{2}. \end{aligned}$$

Proof. To start, we have that

$$\begin{aligned} & \langle \nabla f(\mathbf{x}_t), \nabla f(\mathbf{x}_t) - \mathbf{g}_t(\mathbf{x}_{t+\frac{1}{2}}) \rangle \\ &= \langle \nabla f(\mathbf{x}_t), \nabla f(\mathbf{x}_t) - \mathbf{g}_t(\mathbf{x}_t) + \mathbf{g}_t(\mathbf{x}_t) - \mathbf{g}_t(\mathbf{x}_{t+\frac{1}{2}}) \rangle. \end{aligned}$$

Taking expectation conditioned on \mathbf{x}_t , we arrive at

$$\begin{aligned} & \mathbb{E}[\langle \nabla f(\mathbf{x}_t), \nabla f(\mathbf{x}_t) - \mathbf{g}_t(\mathbf{x}_{t+\frac{1}{2}}) \rangle | \mathbf{x}_t] \\ &= \mathbb{E}[\langle \nabla f(\mathbf{x}_t), \nabla f(\mathbf{x}_t) - \mathbf{g}_t(\mathbf{x}_t) \rangle | \mathbf{x}_t] \\ & \quad + \mathbb{E}[\langle \nabla f(\mathbf{x}_t), \mathbf{g}_t(\mathbf{x}_t) - \mathbf{g}_t(\mathbf{x}_{t+\frac{1}{2}}) \rangle | \mathbf{x}_t] \\ &= \mathbb{E}[\langle \nabla f(\mathbf{x}_t), \mathbf{g}_t(\mathbf{x}_t) - \mathbf{g}_t(\mathbf{x}_{t+\frac{1}{2}}) \rangle | \mathbf{x}_t] \\ &\leq \mathbb{E}[\|\nabla f(\mathbf{x}_t)\| \cdot \|\mathbf{g}_t(\mathbf{x}_t) - \mathbf{g}_t(\mathbf{x}_{t+\frac{1}{2}})\| | \mathbf{x}_t] \\ &\stackrel{(a)}{\leq} L \mathbb{E}[\|\nabla f(\mathbf{x}_t)\| \cdot \|\mathbf{x}_t - \mathbf{x}_{t+\frac{1}{2}}\| | \mathbf{x}_t] \\ &\stackrel{(b)}{=} L\rho \|\nabla f(\mathbf{x}_t)\| \end{aligned}$$

where (a) follows from Assumption 2; and (b) holds because $\mathbf{x}_t - \mathbf{x}_{t+\frac{1}{2}} = -\epsilon_t$, and its norm equals ρ . This inequality ensures that

$$\begin{aligned} & \eta_t \mathbb{E}[\langle \nabla f(\mathbf{x}_t), \nabla f(\mathbf{x}_t) - \mathbf{g}_t(\mathbf{x}_{t+\frac{1}{2}}) \rangle | \mathbf{x}_t] \\ & \leq L\rho \eta_t \|\nabla f(\mathbf{x}_t)\| \leq \frac{L\eta_t^2 \|\nabla f(\mathbf{x}_t)\|^2}{2} + \frac{L\rho^2}{2} \end{aligned}$$

where the last inequality holds because $\rho \eta_t \|\nabla f(\mathbf{x}_t)\| \leq \frac{1}{2} \eta_t^2 \|\nabla f(\mathbf{x}_t)\|^2 + \frac{1}{2} \rho^2$. Taking expectation w.r.t. \mathbf{x}_t completes the proof. \square

Lemma 2. Alg. 1 (or equivalently iteration (8)) ensures that

$$\mathbb{E}[\|\mathbf{g}_t(\mathbf{x}_{t+\frac{1}{2}})\|^2] \leq 2L^2\rho^2 + 2\mathbb{E}[\|\nabla f(\mathbf{x}_t)\|^2] + 2\sigma^2.$$

Proof. The proof starts with bounding $\|\mathbf{g}_t(\mathbf{x}_{t+\frac{1}{2}})\|$ as

$$\begin{aligned} \|\mathbf{g}_t(\mathbf{x}_{t+\frac{1}{2}})\|^2 &= \|\mathbf{g}_t(\mathbf{x}_{t+\frac{1}{2}}) - \mathbf{g}_t(\mathbf{x}_t) + \mathbf{g}_t(\mathbf{x}_t)\|^2 \\ &\leq 2\|\mathbf{g}_t(\mathbf{x}_{t+\frac{1}{2}}) - \mathbf{g}_t(\mathbf{x}_t)\|^2 + 2\|\mathbf{g}_t(\mathbf{x}_t)\|^2 \\ &\stackrel{(a)}{\leq} 2L^2\|\mathbf{x}_t - \mathbf{x}_{t+\frac{1}{2}}\|^2 + 2\|\mathbf{g}_t(\mathbf{x}_t)\|^2 \\ &\stackrel{(b)}{=} 2L^2\rho^2 + 2\|\mathbf{g}_t(\mathbf{x}_t) - \nabla f(\mathbf{x}_t) + \nabla f(\mathbf{x}_t)\|^2 \end{aligned}$$

where (a) follows from Assumption 2; and (b) is because $\mathbf{x}_t - \mathbf{x}_{t+\frac{1}{2}} = -\epsilon_t$, and its norm equals ρ .

Taking expectation conditioned on \mathbf{x}_t , we have

$$\begin{aligned} & \mathbb{E}[\|\mathbf{g}_t(\mathbf{x}_{t+\frac{1}{2}})\|^2 | \mathbf{x}_t] \\ & \leq 2L^2\rho^2 + 2\mathbb{E}[\|\mathbf{g}_t(\mathbf{x}_t) - \nabla f(\mathbf{x}_t) + \nabla f(\mathbf{x}_t)\|^2 | \mathbf{x}_t] \\ & \leq 2L^2\rho^2 + 2\|\nabla f(\mathbf{x}_t)\|^2 + 2\sigma^2 \end{aligned}$$

where the last inequality is because of Assumption 3. Taking expectation w.r.t. the randomness in \mathbf{x}_t completes the proof. \square

Lemma 3. With $A_{t+1} = \alpha A_t + \beta$ for some $\alpha \in (0, 1)$, we have

$$A_{t+1} \leq \alpha^{t+1} A_0 + \frac{\beta}{1-\alpha}.$$

Proof. The proof can be completed by simply unrolling A_{t+1} and using the fact that $1 + \alpha + \alpha^2 + \dots + \alpha^t \leq \frac{1}{1-\alpha}$. \square

D.2 Proof of Theorem 1

Proof. Using Assumption 2, we have that

$$\begin{aligned}
& f(\mathbf{x}_{t+1}) - f(\mathbf{x}_t) \\
& \leq \langle \nabla f(\mathbf{x}_t), \mathbf{x}_{t+1} - \mathbf{x}_t \rangle + \frac{L}{2} \|\mathbf{x}_{t+1} - \mathbf{x}_t\|^2 \\
& = -\eta_t \langle \nabla f(\mathbf{x}_t), \mathbf{g}_t(\mathbf{x}_{t+\frac{1}{2}}) \rangle + \frac{L\eta_t^2}{2} \|\mathbf{g}_t(\mathbf{x}_{t+\frac{1}{2}})\|^2 \\
& = -\eta_t \langle \nabla f(\mathbf{x}_t), \mathbf{g}_t(\mathbf{x}_{t+\frac{1}{2}}) - \nabla f(\mathbf{x}_t) + \nabla f(\mathbf{x}_t) \rangle \\
& \quad + \frac{L\eta_t^2}{2} \|\mathbf{g}_t(\mathbf{x}_{t+\frac{1}{2}})\|^2 \\
& = -\eta_t \|\nabla f(\mathbf{x}_t)\|^2 - \eta_t \langle \nabla f(\mathbf{x}_t), \mathbf{g}_t(\mathbf{x}_{t+\frac{1}{2}}) - \nabla f(\mathbf{x}_t) \rangle \\
& \quad + \frac{L\eta_t^2}{2} \|\mathbf{g}_t(\mathbf{x}_{t+\frac{1}{2}})\|^2.
\end{aligned}$$

Taking expectation, and plugging Lemmas 1 and 2, yields

$$\begin{aligned}
\mathbb{E}[f(\mathbf{x}_{t+1}) - f(\mathbf{x}_t)] & \leq -\left(\eta_t - \frac{3L\eta_t^2}{2}\right) \mathbb{E}[\|\nabla f(\mathbf{x}_t)\|^2] \\
& \quad + \frac{L\rho^2}{2} + L^3\eta_t^2\rho^2 + L\eta_t^2\sigma^2.
\end{aligned}$$

As the parameter selection ensures that $\eta_t \equiv \eta = \frac{\eta_0}{\sqrt{T}} \leq \frac{2}{3L}$, we can divide both sides by η , and rearrange terms to arrive at

$$\begin{aligned}
& \left(1 - \frac{3L\eta}{2}\right) \mathbb{E}[\|\nabla f(\mathbf{x}_t)\|^2] \\
& \leq \frac{\mathbb{E}[f(\mathbf{x}_t) - f(\mathbf{x}_{t+1})]}{\eta} + \frac{L\rho^2}{2\eta} + L^3\eta\rho^2 + L\eta\sigma^2.
\end{aligned}$$

Summing over t , we have

$$\begin{aligned}
& \left(1 - \frac{3L\eta}{2}\right) \frac{1}{T} \sum_{t=0}^{T-1} \mathbb{E}[\|\nabla f(\mathbf{x}_t)\|^2] \\
& \leq \frac{\mathbb{E}[f(\mathbf{x}_0) - f(\mathbf{x}_T)]}{\eta T} + \frac{L\rho^2}{2\eta} + L^3\eta\rho^2 + L\eta\sigma^2 \\
& \stackrel{(a)}{\leq} \frac{f(\mathbf{x}_0) - f^*}{\eta T} + \frac{L\rho^2}{2\eta} + L^3\eta\rho^2 + L\eta\sigma^2 \\
& = \frac{f(\mathbf{x}_0) - f^*}{\eta_0\sqrt{T}} + \frac{L\rho_0^2}{2\eta_0\sqrt{T}} + \frac{L^3\eta_0\rho_0^2}{T^{3/2}} + \frac{L\eta_0\sigma^2}{\sqrt{T}}
\end{aligned}$$

where (a) uses Assumption 1, and the last equality is obtained by plugging in the values of ρ and η . This completes the proof of the first part.

For the second part of this theorem, we have that

$$\begin{aligned}
& \mathbb{E}[\|\nabla f(\mathbf{x}_t + \boldsymbol{\epsilon}_t)\|^2] \\
& = \mathbb{E}[\|\nabla f(\mathbf{x}_t + \boldsymbol{\epsilon}_t) + \nabla f(\mathbf{x}_t) - \nabla f(\mathbf{x}_t)\|^2] \\
& \leq 2\mathbb{E}[\|\nabla f(\mathbf{x}_t)\|^2] + 2\mathbb{E}[\|\nabla f(\mathbf{x}_t + \boldsymbol{\epsilon}_t) - \nabla f(\mathbf{x}_t)\|^2] \\
& \leq 2\mathbb{E}[\|\nabla f(\mathbf{x}_t)\|^2] + 2L^2\rho^2 \\
& = 2\mathbb{E}[\|\nabla f(\mathbf{x}_t)\|^2] + \frac{2L^2\rho_0^2}{T}.
\end{aligned}$$

Averaging over t completes the proof.

Extension. Theorem 1 also holds when $\boldsymbol{\epsilon}_t \in \mathbb{S}_\rho(\mathbf{0})$ is replaced by $\boldsymbol{\epsilon}_t \in \mathbb{B}_\rho(\mathbf{0})$. Since the derivation is similar, we will skip it here. \square

D.3 Proof of Theorem 2

Proof. To bound the MSE, we first have that

$$\begin{aligned}
& \|\mathbf{d}_t - \nabla f(\mathbf{x}_t)\|^2 \\
& = \|(1-\theta)\mathbf{d}_{t-1} + \theta\mathbf{g}_t(\mathbf{x}_t) - (1-\theta)\nabla f(\mathbf{x}_t) - \theta\nabla f(\mathbf{x}_t)\|^2 \\
& = (1-\theta)^2 \|\mathbf{d}_{t-1} - \nabla f(\mathbf{x}_t)\|^2 + \theta^2 \|\mathbf{g}_t(\mathbf{x}_t) - \nabla f(\mathbf{x}_t)\|^2 \\
& \quad + 2\theta(1-\theta) \langle \mathbf{d}_{t-1} - \nabla f(\mathbf{x}_t), \mathbf{g}_t(\mathbf{x}_t) - \nabla f(\mathbf{x}_t) \rangle.
\end{aligned} \tag{9}$$

We will cope with three terms in the right hand side (rhs) of (9) separately.

The second term can be bounded directly using Assumption 2

$$\mathbb{E}[\|\mathbf{g}_t(\mathbf{x}_t) - \nabla f(\mathbf{x}_t)\|^2 | \mathbf{x}_t] \leq \sigma^2. \tag{10}$$

For the third term, we have

$$\mathbb{E}[\langle \mathbf{d}_{t-1} - \nabla f(\mathbf{x}_t), \mathbf{g}_t(\mathbf{x}_t) - \nabla f(\mathbf{x}_t) \rangle | \mathbf{x}_t] = 0. \tag{11}$$

The first term is bounded through

$$\begin{aligned}
& \|\mathbf{d}_{t-1} - \nabla f(\mathbf{x}_t)\|^2 \\
& = \|\mathbf{d}_{t-1} - \nabla f(\mathbf{x}_{t-1}) + \nabla f(\mathbf{x}_{t-1}) - \nabla f(\mathbf{x}_t)\|^2 \\
& \stackrel{(a)}{\leq} (1+\lambda) \|\mathbf{d}_{t-1} - \nabla f(\mathbf{x}_{t-1})\|^2 + (1+\frac{1}{\lambda}) \|\nabla f(\mathbf{x}_{t-1}) - \nabla f(\mathbf{x}_t)\|^2 \\
& \leq (1+\lambda) \|\mathbf{d}_{t-1} - \nabla f(\mathbf{x}_{t-1})\|^2 + (1+\frac{1}{\lambda}) L^2 \|\mathbf{x}_{t-1} - \mathbf{x}_t\|^2 \\
& = (1+\lambda) \|\mathbf{d}_{t-1} - \nabla f(\mathbf{x}_{t-1})\|^2 + (1+\frac{1}{\lambda}) \eta^2 L^2 \|\mathbf{g}_{t-1}(\mathbf{x}_{t-\frac{1}{2}})\|^2
\end{aligned}$$

where (a) follows from Young's inequality. Taking expectation and applying Lemma 2, we arrive at

$$\begin{aligned}
& \mathbb{E}[\|\mathbf{d}_{t-1} - \nabla f(\mathbf{x}_t)\|^2] \\
& \leq (1+\lambda) \mathbb{E}[\|\mathbf{d}_{t-1} - \nabla f(\mathbf{x}_{t-1})\|^2] \\
& \quad + (1+\frac{1}{\lambda}) \eta^2 L^2 \left(2L^2\rho^2 + 2\mathbb{E}[\|\nabla f(\mathbf{x}_{t-1})\|^2] + 2\sigma^2 \right) \\
& \leq (1+\lambda) \mathbb{E}[\|\mathbf{d}_{t-1} - \nabla f(\mathbf{x}_{t-1})\|^2] + (1+\frac{1}{\lambda}) \cdot \mathcal{O}\left(\frac{\sigma^2}{\sqrt{T}}\right).
\end{aligned} \tag{12}$$

The last inequality uses the value of $\eta = \frac{\eta_0}{\sqrt{T}}$ and $\rho = \frac{\rho_0}{\sqrt{T}}$. In particular, we have $\eta^2\rho^2L^4 = \mathcal{O}(1/T^2)$ and $\eta^2L^2\sigma^2 = \mathcal{O}(\sigma^2/T)$, and

$$\begin{aligned}
& \eta^2 L^2 \mathbb{E}[\|\nabla f(\mathbf{x}_t)\|^2] = \frac{\eta_0^2 L^2}{T} \mathbb{E}[\|\nabla f(\mathbf{x}_t)\|^2] \\
& \leq \eta_0^2 L^2 \frac{1}{T} \sum_{t=0}^{T-1} \mathbb{E}[\|\nabla f(\mathbf{x}_t)\|^2] = \mathcal{O}\left(\frac{\sigma^2}{\sqrt{T}}\right)
\end{aligned}$$

where for the last equality we have also used Theorem 1.

Combining (9) with (12), (10) with (11), and choosing $\lambda = \frac{\theta}{1-\theta}$, we have

$$\begin{aligned}
& \mathbb{E}[\|\mathbf{d}_t - \nabla f(\mathbf{x}_t)\|^2] \\
& \leq (1-\theta) \mathbb{E}[\|\mathbf{d}_{t-1} - \nabla f(\mathbf{x}_{t-1})\|^2] + \frac{(1-\theta)^2}{\theta} \mathcal{O}\left(\frac{\sigma^2}{\sqrt{T}}\right) + \theta^2 \sigma^2 \\
& \leq \theta \sigma^2 + \mathcal{O}\left(\frac{(1-\theta)^2 \sigma^2}{\theta^2 \sqrt{T}}\right)
\end{aligned}$$

where the last inequality is the result of Lemma 3. \square

D.4 Proof of Theorem 3

Proof. We adopt a unified notation for simplicity. Let $\mathbf{v}_t := \mathbf{d}_t$ for VASSO, and $\mathbf{v}_t := \mathbf{g}_t(\mathbf{x}_t)$ for SAM. Then for both VASSO and SAM, we can write

$$\begin{aligned} f(\mathbf{x}_t) + \langle \mathbf{v}_t, \boldsymbol{\epsilon}_t \rangle &= f(\mathbf{x}_t) + \rho \|\mathbf{v}_t\| \\ &= f(\mathbf{x}_t) + \rho \|\mathbf{v}_t - \nabla f(\mathbf{x}_t) + \nabla f(\mathbf{x}_t)\|. \end{aligned} \quad (13)$$

For convenience, let $\boldsymbol{\epsilon}_t^* = \rho \nabla f(\mathbf{x}_t) / \|\nabla f(\mathbf{x}_t)\|$. From (13), we have that

$$\begin{aligned} f(\mathbf{x}_t) + \langle \mathbf{v}_t, \boldsymbol{\epsilon}_t \rangle &= f(\mathbf{x}_t) + \rho \|\mathbf{v}_t - \nabla f(\mathbf{x}_t) + \nabla f(\mathbf{x}_t)\| \\ &\leq f(\mathbf{x}_t) + \rho \|\nabla f(\mathbf{x}_t)\| + \rho \|\mathbf{v}_t - \nabla f(\mathbf{x}_t)\| \\ &= f(\mathbf{x}_t) + \langle \nabla f(\mathbf{x}_t), \boldsymbol{\epsilon}_t^* \rangle + \rho \|\mathbf{v}_t - \nabla f(\mathbf{x}_t)\|. \end{aligned} \quad (14)$$

Applying the triangle inequality $\|\mathbf{a}\| - \|\mathbf{b}\| \leq \|\mathbf{a} - \mathbf{b}\|$, we arrive at

$$\begin{aligned} f(\mathbf{x}_t) + \langle \mathbf{v}_t, \boldsymbol{\epsilon}_t \rangle &= f(\mathbf{x}_t) + \rho \|\nabla f(\mathbf{x}_t) - (\nabla f(\mathbf{x}_t) - \mathbf{v}_t)\| \\ &\geq f(\mathbf{x}_t) + \rho \|\nabla f(\mathbf{x}_t)\| - \rho \|\mathbf{v}_t - \nabla f(\mathbf{x}_t)\| \\ &= f(\mathbf{x}_t) + \langle \nabla f(\mathbf{x}_t), \boldsymbol{\epsilon}_t^* \rangle - \rho \|\mathbf{v}_t - \nabla f(\mathbf{x}_t)\|. \end{aligned} \quad (15)$$

Combining (14) with (15), we have

$$|\mathcal{L}_t(\mathbf{v}_t) - \mathcal{L}_t(\nabla f(\mathbf{x}_t))| \leq \rho \|\mathbf{v}_t - \nabla f(\mathbf{x}_t)\|$$

which further implies that

$$\begin{aligned} \mathbb{E}[|\mathcal{L}_t(\mathbf{v}_t) - \mathcal{L}_t(\nabla f(\mathbf{x}_t))|] &\leq \rho \mathbb{E}[\|\mathbf{v}_t - \nabla f(\mathbf{x}_t)\|] \\ &\leq \rho \sqrt{\mathbb{E}[\|\mathbf{v}_t - \nabla f(\mathbf{x}_t)\|^2]} \end{aligned}$$

where the last inequality follows from $(\mathbb{E}[a])^2 \leq \mathbb{E}[a^2]$. This theorem can be proved by applying Assumption 3 for SAM, and Lemma 2 for VASSO. \square

D.5 Proof for Theorem 4

We start with a technical lemma needed for the main theorem.

Lemma 4. Alg. 2 ensures that

$$\mathbb{E}[\|\mathbf{g}_t(\mathbf{x}_t + \boldsymbol{\epsilon}_t)\|^2] \leq 2pL^2\rho^2 + (1+p)\|\nabla f(\mathbf{x}_t)\|^2 + (1+p)\sigma^2.$$

Proof. First, consider the case where $B_t = 1$. We have that

$$\begin{aligned} \|\mathbf{g}_t(\mathbf{x}_t + \boldsymbol{\epsilon}_t)\|^2 &= \|\mathbf{g}_t(\mathbf{x}_t + \boldsymbol{\epsilon}_t) - \mathbf{g}_t(\mathbf{x}_t) + \mathbf{g}_t(\mathbf{x}_t)\|^2 \\ &\leq 2\|\mathbf{g}_t(\mathbf{x}_t + \boldsymbol{\epsilon}_t) - \mathbf{g}_t(\mathbf{x}_t)\|^2 + 2\|\mathbf{g}_t(\mathbf{x}_t)\|^2 \\ &\stackrel{(a)}{\leq} 2L^2\|\boldsymbol{\epsilon}_t\|^2 + 2\|\mathbf{g}_t(\mathbf{x}_t)\|^2 \\ &\stackrel{(b)}{=} 2L^2\rho^2 + 2\|\mathbf{g}_t(\mathbf{x}_t) - \nabla f(\mathbf{x}_t) + \nabla f(\mathbf{x}_t)\|^2 \end{aligned}$$

where (a) is due to Assumption 2; and (b) is because $\|\boldsymbol{\epsilon}_t\| = \rho$.

When $B_t = 0$, i.e., $\boldsymbol{\epsilon}_t = \mathbf{0}$, we have that

$$\|\mathbf{g}_t(\mathbf{x}_t + \boldsymbol{\epsilon}_t)\|^2 = \|\mathbf{g}_t(\mathbf{x}_t)\|^2 = \|\mathbf{g}_t(\mathbf{x}_t) - \nabla f(\mathbf{x}_t) + \nabla f(\mathbf{x}_t)\|^2.$$

Taking expectation conditioned on \mathbf{x}_t , we have

$$\begin{aligned} &\mathbb{E}[\|\mathbf{g}_t(\mathbf{x}_t + \boldsymbol{\epsilon}_t)\|^2 | \mathbf{x}_t] \\ &\leq 2pL^2\rho^2 + (1+p)\mathbb{E}[\|\mathbf{g}_t(\mathbf{x}_t) - \nabla f(\mathbf{x}_t) + \nabla f(\mathbf{x}_t)\|^2 | \mathbf{x}_t] \\ &\leq 2pL^2\rho^2 + (1+p)\|\nabla f(\mathbf{x}_t)\|^2 + (1+p)\sigma^2 \end{aligned}$$

where the last inequality is because of Assumption 3. Taking expectation w.r.t. the randomness in \mathbf{x}_t completes the proof. \square

Now we are ready to prove Theorem 4.

Proof. Similar to (9), we have that for eVASSO

$$\begin{aligned} \|\mathbf{d}_t - \nabla f(\mathbf{x}_t)\|^2 &= (1-\theta)^2 \|\mathbf{d}_{t-1} - \nabla f(\mathbf{x}_t)\|^2 + \theta^2 \|\mathbf{g}_t(\mathbf{x}_t) - \nabla f(\mathbf{x}_t)\|^2 \\ &\quad + 2\theta(1-\theta) \langle \mathbf{d}_{t-1} - \nabla f(\mathbf{x}_t), \mathbf{g}_t(\mathbf{x}_t) - \nabla f(\mathbf{x}_t) \rangle. \end{aligned} \quad (16)$$

Again, we deal with the three terms in the rhs (16) separately.

The second term can be bounded directly using Assumption 2

$$\mathbb{E}[\|\mathbf{g}_t(\mathbf{x}_t) - \nabla f(\mathbf{x}_t)\|^2 | \mathbf{x}_t] \leq \sigma^2. \quad (17)$$

For the third term, we have

$$\mathbb{E}[\langle \mathbf{d}_{t-1} - \nabla f(\mathbf{x}_t), \mathbf{g}_t(\mathbf{x}_t) - \nabla f(\mathbf{x}_t) \rangle | \mathbf{x}_t] = 0. \quad (18)$$

The first term is bounded through

$$\begin{aligned} \|\mathbf{d}_{t-1} - \nabla f(\mathbf{x}_t)\|^2 &= \|\mathbf{d}_{t-1} - \nabla f(\mathbf{x}_{t-1}) + \nabla f(\mathbf{x}_{t-1}) - \nabla f(\mathbf{x}_t)\|^2 \\ &\stackrel{(a)}{\leq} (1+\lambda) \|\mathbf{d}_{t-1} - \nabla f(\mathbf{x}_{t-1})\|^2 + (1+\frac{1}{\lambda}) \|\nabla f(\mathbf{x}_{t-1}) - \nabla f(\mathbf{x}_t)\|^2 \\ &\leq (1+\lambda) \|\mathbf{d}_{t-1} - \nabla f(\mathbf{x}_{t-1})\|^2 + (1+\frac{1}{\lambda}) L^2 \|\mathbf{x}_{t-1} - \mathbf{x}_t\|^2 \\ &= (1+\lambda) \|\mathbf{d}_{t-1} - \nabla f(\mathbf{x}_{t-1})\|^2 + (1+\frac{1}{\lambda}) \eta^2 L^2 \|\mathbf{g}_{t-1}(\mathbf{x}_{t-1} + \boldsymbol{\epsilon}_{t-1})\|^2 \end{aligned}$$

where (a) follows from Young's inequality. Taking expectation and applying Lemma 4, we deduce that

$$\begin{aligned} &\mathbb{E}[\|\mathbf{d}_{t-1} - \nabla f(\mathbf{x}_t)\|^2] \\ &\leq (1+\lambda) \mathbb{E}[\|\mathbf{d}_{t-1} - \nabla f(\mathbf{x}_{t-1})\|^2] \\ &\quad + (1+\frac{1}{\lambda}) \eta^2 L^2 \left(2pL^2\rho^2 + (1+p) \mathbb{E}[\|\nabla f(\mathbf{x}_{t-1})\|^2] \right) \\ &\quad + (1+\frac{1}{\lambda}) \eta^2 L^2 (1+p) \sigma^2 \\ &\leq (1+\lambda) \mathbb{E}[\|\mathbf{d}_{t-1} - \nabla f(\mathbf{x}_{t-1})\|^2] + (1+\frac{1}{\lambda}) \cdot \mathcal{O}\left(\frac{\sigma^2}{\sqrt{T}}\right). \end{aligned} \quad (19)$$

The last inequality uses the values of $\eta = \frac{\eta_0}{\sqrt{T}}$ and $\rho = \frac{\rho_0}{\sqrt{T}}$. In particular, we have $\eta^2 \rho^2 L^4 = \mathcal{O}(1/T^2)$ and $\eta^2 L^2 \sigma^2 = \mathcal{O}(\sigma^2/T)$, and

$$\begin{aligned} \eta^2 L^2 \mathbb{E}[\|\nabla f(\mathbf{x}_t)\|^2] &= \frac{\eta_0^2 L^2}{T} \mathbb{E}[\|\nabla f(\mathbf{x}_t)\|^2] \\ &\leq \eta_0^2 L^2 \frac{1}{T} \sum_{t=0}^{T-1} \mathbb{E}[\|\nabla f(\mathbf{x}_t)\|^2] = \mathcal{O}\left(\frac{\sigma^2}{\sqrt{T}}\right) \end{aligned}$$

where the last equation is the result of Theorem 1.

Combining (16) with (19), (17) with (18), and choosing $\lambda = \frac{\theta}{1-\theta}$, we have

$$\begin{aligned} &\mathbb{E}[\|\mathbf{d}_t - \nabla f(\mathbf{x}_t)\|^2] \\ &\leq (1-\theta) \mathbb{E}[\|\mathbf{d}_{t-1} - \nabla f(\mathbf{x}_{t-1})\|^2] + \frac{(1-\theta)^2}{\theta} \mathcal{O}\left(\frac{\sigma^2}{\sqrt{T}}\right) + \theta^2 \sigma^2 \\ &\leq \theta \sigma^2 + \mathcal{O}\left(\frac{(1-\theta)^2 \sigma^2}{\theta^2 \sqrt{T}}\right) \end{aligned}$$

where the last inequality is the result of Lemma 3. \square